Strength of the H2O near-infrared absorption bands in hydrated minerals: Effects of particle size and correlation with albedo

Antoine Pommerol, Bernard Schmitt

Strength of the H_2O near-infrared absorption bands in hydrated minerals: Effects of particle size and correlation with albedo

Antoine Pommerol[1] and Bernard Schmitt[1]

Received 26 December 2007; revised 22 July 2008; accepted 9 July 2008; published 22 October 2008.

[1] We use laboratory experiments and radiative transfer modeling to study how the 1.9- and 3-μm H_2O absorption bands are affected by variations of mineral particle size and albedo. A consistency between results of physical experiments and numerical simulations demonstrates that the studied effects are well described by the theory of radiative transfer in particulate media. Band strengths show different relationships with particle size, depending on the absolute intensity of the absorption and the criterion used to calculate band strength (band depth, area, ESPAT function, etc.). Various mixing processes used to vary sample albedo reveal a strong dependence of band strengths with albedo. For the 1.9-μm band, those effects result in variations of the hydrated minerals detection limit by more than 1 order of magnitude. However, the shape of the relationship between the 1.9-μm band strength and albedo could be used to get information on the mixing mode (intimate, granular, or geographic) between hydrated and nonhydrated minerals. For the 3-μm band, we found a strong linear correlation between the integrated band area and the continuum reflectance that opens a promising way to isolate the effect of albedo on planetary surfaces and retrieve spatial variations of material hydration state. When this spectral criterion is used for the 3-μm band, the effects of particle size are very limited for particles larger than 150 μm but remain important below this value. Therefore, an independent way to derive particle size from remote sensing appears necessary to address the effects of particle size variations where small particles are present.

Citation: Pommerol, A., and B. Schmitt (2008), Strength of the H_2O near-infrared absorption bands in hydrated minerals: Effects of particle size and correlation with albedo, *J. Geophys. Res.*, *113*, E10009, doi:10.1029/2007JE003069.

1. Introduction

[2] Hydrated minerals are observed on the surface of different solar system objects. Minerals containing water in various forms are observed at the surface of some terrestrial planets, asteroids, giant planets satellites, as well as other outer solar system bodies. The different kinds of interaction between minerals and water, regrouped under the term "hydrated minerals," give important clues about the role of water during the geological history of these objects. Near-infrared reflectance spectroscopy (1–5 μm) is particularly useful to study mineral hydration on planetary surfaces because the presence of water produces strong absorption bands in this spectral range. Two fundamental vibration modes (symmetric and asymmetric stretching: ν_1 and ν_3) and one overtone mode (bending: 2 ν_2) of the water molecule are responsible for a strong absorption band located at about 3 μm. Weaker absorption bands located around 1.4 and 1.9 μm are respectively attributed to overtone and combination modes $\nu_1 + \nu_3$, 2 ν_1, 2 ν_3, $\nu_1 +$ 2 ν_2, and $\nu_3 + 2\ \nu_2$ [*Ockman*, 1958] and to the banding plus stretching combination ($\nu + \nu_2$) modes of the water molecule [*Ryskin*, 1974].

[3] A large diversity of hydrated minerals can be found on Earth and the 1.4-, 1.9-, and 3-μm absorption bands can be easily observed in laboratory measurements. The strong and broad 3-μm band can be observed in the reflectance spectra of virtually all the minerals under ambient atmospheric conditions because of adsorption of water vapor onto mineral surfaces, whereas the presence of the 1.4- and 1.9-μm bands requires larger amounts of water. Therefore, these weaker bands are particularly intense in minerals containing structural water (sulfates, etc.), or "solvation water" trapped into particular mineralogical sites (phyllosilicates, zeolites, etc.) but can also be due to water adsorbed on the surface of hygroscopic minerals that present large adsorption areas.

1.1. Observation of Hydration Bands on Solar System Objects Surfaces

1.1.1. Mars

[4] Except for the Earth, Mars is the first object of the solar system where mineral hydration was detected through the observation of the 3-μm band from telescopic observations [*Moroz*, 1964]. The depth of this strong band has then been mapped over portions of the Martian surface by the IRS spectrometer (Mariner 6 and7) [*Calvin*, 1997] and by the ISM imaging spectrometer (Phobos 2) [*Murchie et al.*,

[1]Laboratoire de Planétologie de Grenoble, Université Joseph Fourier, CNRS/INSU, Grenoble, France.

0148-0227/08/2007JE003069

2000]. A comparison of the results obtained from these two data sets can be found in the work by *Erard and Calvin* [1997]. Since January 2004, the imaging spectrometer OMEGA [*Bibring et al.*, 2004] on board ESA Mars Express spacecraft has mapped the whole Martian surface between 0.3 and 5.1 μm at various spatial resolutions. This new data set has been used to produce global maps of the 3-μm band depth [*Jouglet et al.*, 2007; *Milliken et al.*, 2007] and to derive maps of the surface material absolute water content using empirical relations between band strength and absolute water content [*Milliken et al.*, 2007]. The first important result of this global study is the presence of the 3-μm absorption everywhere on the surface [*Jouglet et al.*, 2007]. Spatial variations of the 3-μm band depth show a global, strong, and positive correlation with albedo within all the data sets (IRS, ISM, and OMEGA) as well as strong local variations, not always correlated with albedo. The weaker 1.4- and 1.9-μm bands have also been observed on local areas of the Martian surface thanks to the OMEGA data set [*Bibring et al.*, 2006]. In some cases, hydrated minerals (sulfates and phyllosilicates) responsible of these absorptions have been identified [*Bibring et al.*, 2005; *Gendrin et al.*, 2005; *Langevin et al.*, 2005; *Poulet et al.*, 2005]. *Bibring et al.* [2006] published a global map of hydrated minerals built from the 1.9-μm band detection and observation of other weak absorption bands in the near infrared. They used this global map to discuss the role of water during the planet geological history. From a telescopic observation conducted with the NICMOS instrument on board the Hubble Space Telescope, *Noe Dobrea et al.* [2003] also published a hemispheric map of the 1.4- and 1.9-μm hydration band depths that shows the spatial variability of these bands.

1.1.2. Asteroids

[5] The presence of hydrated minerals at the surface of some classes of asteroids is well established thanks to laboratory studies of meteorites and remote sensing observations of asteroids. In a recent paper, *Rivkin et al.* [2003] review previous studies of hydrated minerals on C-class asteroids. They also present a new method to estimate the hydrogen concentration on C-class asteroid surfaces based on the comparison of the 3-μm band strength measured on asteroid surfaces and experimental results on carbonaceous chondrites obtained by *Miyamoto and Zolensky* [1994] and *Sato et al.* [1997]. *Hasegawa et al.* [2003] identified hydrated and/or hydroxylated minerals on the surface of the asteroid 4-Vesta thanks to the observation of a weak 3-μm absorption feature. However, this identification was not confirmed by further observations [*Rivkin et al.*, 2006].

1.1.3. Outer Solar System Objects

[6] Hydrated minerals were also detected, and sometimes identified, at the surface of some outer solar system icy bodies. *Calvin and Clark* [1993] observed an absorption between 3 and 4.3 μm in Callisto's surface spectra that they attributed to hydrated minerals. *McCord et al.* [1999] suggested heavily hydrated salt minerals on Europa's surface from Galileo/NIMS spectral data. However, sulphuric acid hydrate can also explain those spectral features [*Carlson et al.*, 2005]. *Vilas et al.* [2006] used the 0.7-μm Fe^{2+}/Fe^{3+} absorption band as a proxy of the 3-μm band to detect hydrated minerals on the surfaces of different irregular outer planets satellites. Hydrated minerals were also potentially detected at the surface of two plutinos by *De Bergh et al.* [2004].

1.2. Band Strength and Water Content

[7] The simple detection of one of the H_2O absorption bands in the surface spectra of a given object indicates that frosts or hydrated minerals lie among the surface components. The observation of the 1.9-μm band indicates the presence of H_2O, while the observation of the 1.4 and 3-μm band only indicates the presence of OH [*Clark et al.*, 1990]. But the information contained in the reflectance spectra could potentially be used in a more quantitative way. Important information that could be extracted from reflectance spectra is the amount of water trapped into the surface material. This would also permit the comparison of the hydration states between the surfaces of different objects or between different areas of the same surface. Several experimental studies have already been conducted to determine an empirical relationship between the strength of the hydration bands and the sample water content.

[8] *Miyamoto and Zolensky* [1994] measured near-infrared reflectance spectra of carbonaceous meteorites and determined the correlation between the integrated intensity of the 3-μm absorption band and the ratio between hydrogen and silicon elemental abundances in the meteorite samples. Considering that a simple band depth at one given wavelength inside the broad 3-μm band is correlated with the band integrated intensity [*Sato et al.*, 1997], *Rivkin et al.* [2003] used empirical relationships between band depths at 2.9 and 3.2 μm and the H/Si ratio derived from these experimental studies to determine the H/Si ratio of different C-class asteroid surfaces. *Yen et al.* [1998] prepared mixtures between hydrated and anhydrous minerals to obtain materials with various hydration states. They proposed an empirical relationship between sample water content and the apparent absorbance ($-\ln$ (reflectance)) at 2.9 μm. These authors selected this criterion instead of the integrated intensity measured on reflectance spectra because the apparent absorbance gives a more linear relationship between band strength and water content and is potentially less sensitive to particle size and packing density variations than parameters directly based on reflectance values. These experimental results led to an estimate of less than 4% of adsorbed and/or bound water in the Martian surface minerals based on Phobos 2/ISM data set. *Whiting et al.* [2004] proposed the Soil Moisture Gaussian Model (SMGM) to estimate soil moisture from hyperspectral observations. This method is based on the fit of an inverted Gaussian function on the 1.2–2.5 μm spectral range (wing of the 2.8-μm fundamental absorption). However, this method is only valid when the soil moisture is large enough for this wing to become significant (a few percent of water by mass, depending on the mineral nature) and is difficult to apply to nonterrestrial soils. Recently, *Milliken and Mustard* [2005] evaluated a number of spectral criteria to identify which one is the most robust in order to determine material water content from near-infrared remote sensing observations. Their experimental procedure consists in heating five types of minerals at very high temperature by small steps to extract the mass loss on heating at each step and the corresponding reflectance spectra. They concluded that the "normalized optical path length" is the most appropriate

parameter to quantify the water content of planetary materials because it is relatively independent from the sample composition. Furthermore, this spectral criterion is directly calculated from reflectance spectra, avoiding any conversion to different units. Another spectral criterion, the ESPAT parameter, also shows a very good correlation with sample water content. However, the calculation of this parameter requires conversion of reflectance spectra to single-scattering albedo. This conversion is only possible if the viewing geometry (incidence and emergence angles) is known. If conversion to single-scattering albedo can be made, ESPAT is preferred to NOPL because it is independent of sample albedo [*Milliken and Mustard*, 2007a].

[9] Unfortunately, extraction of quantitative information from reflectance spectra is particularly challenging because many parameters control the shape and the strength of the absorption bands observed in reflectance. Among these parameters, particle size and shape are the most problematic because they strongly affect surface albedo and spectral contrast between the continuum level and the absorption bands. Measurement geometry (incidence, emergence, azimuth, and phase angles) also affects surface reflectance spectra and absorption band strength.

1.3. Effects of Particle Size

[10] The strong effects of particle size variations on laboratory measured reflectance spectra and especially on band strength has been noted by a number of authors [*Lyon*, 1964; *Aronson et al.*, 1966; *Adams and Felice*, 1967; *Pieters*, 1983; *Hunt*, 1982; *Salisbury and Walter*, 1989; *Salisbury and Wald*, 1992; *Mustard and Hays*, 1997]. *Le Bras and Erard* [2003] conducted a new experimental study with basalt and anorthosite on a wide spectral range (2–40 μm) and a wide range of particle size (25–800 μm). Results of their experimental study are compared with earlier work cited above. In the near infrared, *Le Bras and Erard* [2003] observe different behaviors of the spectral contrast between absorption bands and continuum versus particle size depending on the absolute strength of the absorptions. The strength of the weakest bands decreases in a monotonic way as particle size decreases while the strength of the strongest bands presents a maximum for intermediate sizes as a result of the transition from volume scattering to surface scattering. Those results are in good agreement with other experimental studies [e.g., *Salisbury and Walter*, 1989; *Mustard and Hays*, 1997]. The "3-μm" H_2O band is one of the absorption bands studied by *Le Bras and Erard* [2003]. However, only the simple "band depth" criterion as defined by *Clark and Roush* [1984] is calculated for this band while other spectral criteria are often used to characterize the variations of this band on planetary surfaces as presented in this section. *Cooper and Mustard* [1999] conducted an experimental study to highlight the quantitative effects of particle size variations on the 1.4-, 1.9-, and 2.2-μm hydration band depths for very fine particles. They used two different mineral samples, montmorillonite and palagonite, separated in different grain size fractions varying between less than 5 and 75 μm for the montmorillonite and 250 μm for the palagonite. They observed a strong decrease of band depth when particle size decreases. *Van Keulen et al.* [2000] present reflectance spectra of hydrated salts with different grain sizes between less than 45 and more than 500 μm. These authors noted an increase of continuum reflectance and a decrease of hydration band strengths as particle size decreases. *Yen et al.* [1998], in an experimental study already cited above, concluded that conversion of reflectance spectra to apparent absorbance spectra decreases the effect of particle size on the 3-μm band strength. In a recent paper, *Milliken and Mustard* [2007b] also highlight the effect of particle size variations on the 3-μm band with different samples: nontronite (Fe-rich smectite) and palagonite. The authors tested the different band strength parameters defined by *Milliken and Mustard* [2005]. The particle size variations appeared to have important effects on all these parameters.

1.4. Effects of Albedo and Mixtures

[11] Correlation between the values of hydration band strength and surface or sample albedo has also been a subject of debate by many authors. *Clark* [1983] examined the spectral properties of montmorillonite mixed with dark carbons grains of various sizes. A clear correlation was found between the 1.4-, 1.9-, 2.2-, and 3-μm band strengths and the weight fraction of dark carbon grains introduced in the mixture. For a fixed amount of dark carbon grains in the mixture, band strengths also depend on the carbon grain size. We reproduce a similar experiment in this work but extend the spectral range to a longer wavelength to capture the entire H_2O absorption between 3 and 4 μm. *Milliken and Mustard* [2007a] recently conducted new physical and numerical experiments to highlight this correlation between sample albedo and the 3-μm band strength estimated by the parameters that they previously defined [*Milliken and Mustard*, 2005]. These experiments imply montmorillonite, zeolite, and palagonite as hydrated materials and carbon black and illmenite as darkening agents. They found that the ESPAT parameter is relatively independent of surface albedo. They also discussed the agreement between physical and numerical experiments (linear single-scattering albedo mixing model). This agreement looks good for large darkening grains, but significant discrepancies appear for the smallest grains. However, the ESPAT parameter is defined by *Milliken and Mustard* [2005] at 2.9 μm, the wavelength at which absorption by H_2O is maximum. Therefore, this spectral criterion cannot be used when the absorption band is saturated in this region. In this study, we utilized many minerals that present saturated absorptions in the 2.9-μm region. Thus, we test the ESPAT criterion in the long-wavelength wing of the absorption band as well as other spectral criteria designed to capture variations in the band wing where the band is not saturated.

[12] The question of the correlation between band strength and albedo has especially been discussed in the case of the Martian surface that presents large variations of surface albedo. A strong correlation between the 3-μm band strength estimated by different parameters and surface albedo has been observed using the Mariner 6 and 7/IRS data set [*Calvin*, 1997, 2007], Phobos 2/ISM data set [*Murchie et al.*, 2000], and Mars Express/OMEGA data set [*Jouglet et al.*, 2007; *Milliken et al.*, 2007]. All these authors discuss the possible cause of this correlation with sometimes different interpretations: physical process or a simple bias due to the method of band strength determination. As a result of this correlation, the 3-μm band strength

maps calculated with different parameters display very different patterns.

[13] Different radiative transfer models have been designed to take into account, among other parameters, the effects of grain size and mixtures between materials with different albedo on the continuum reflectance and the absorption bands. Examples of relationships between these parameters calculated by numerical modeling can be found in the works by *Hapke* [1993], *Shkuratov et al.* [1999], and *Shkuratov and Grynko* [2005].

[14] In this study, we present new results regarding the effects of grain size variations and mixtures between materials with different albedo on the 1.9- and 3-μm water of hydration absorption bands. As much as possible, we tried to compare our experimental results with numerical results from radiative transfer modeling. In this way, we test the ability of the radiative transfer modeling code to coherently reproduce behaviors that are observed in the experimental study. Our goal is not to reproduce every aspect of the actual physical experiments using numerical modeling but rather to benefit from the complementary advantages of these two types of approach of the problem.

[15] An upcoming paper, using the same methods and samples, focuses on the effects of measurement geometry (incidence, emergence, phase angles) on the 1.9- and 3-μm water of hydration band strengths (A. Pommerol and B. Schmitt, Strength of the H_2O near-infrared absorption bands in hydrated minerals: Effects of measurement geometry, submitted to *Journal of Geophysical Research*, 2008).

2. Methods

2.1. Experimental Approach

2.1.1. Sample Nature and Preparation

2.1.1.1. Samples

[16] Different samples were prepared and used for each part of the experimental study. For experiments dedicated to investigate the effects of particle size on the absorption band strength, we used a smectite clay purchased from the Clay Minerals Society Source Clay Minerals Repository (sample SWy-2), an altered volcanic tuff collected in Corent (recent volcanic province of Puy de Dôme, France), and an immature coal (PSOC 1532) purchased from the Pennsylvania State University "Coal Sample Bank and Database."

[17] The SWy-2 smectite is a Na-rich montmorillonite. Chemical composition as well as mineralogical information and physical properties are detailed in the special section Baseline studies of the clay minerals society source clays (*Clays and Clay Minerals, 49,* 2001). The sample received from the Source Clay Repository is a heterogeneous powder containing aggregates of different diameters. This powder was dry sieved without any grinding to isolate six particle size fractions: less than 25 μm, 25–50 μm, 50–100 μm, 100–200 μm, 200–280 μm, and 280–400 μm. Figure 1 shows pictures of all different particle size fractions taken on a binocular microscope at three different zoom levels. These pictures reveal the complex shape of the aggregates that are often elongated and relatively far from spheroids. These aggregates are weakly consolidated, as a small pressure applied on them with a spatula is sufficient to divide them in smaller particles. Finally, these aggregates do not appear to be coated by smaller aggregates at the resolution of the microscope. However, we cannot exclude a coating of the large agglomerates by micrometer-sized particles that would not be resolved by the optical microscope we used.

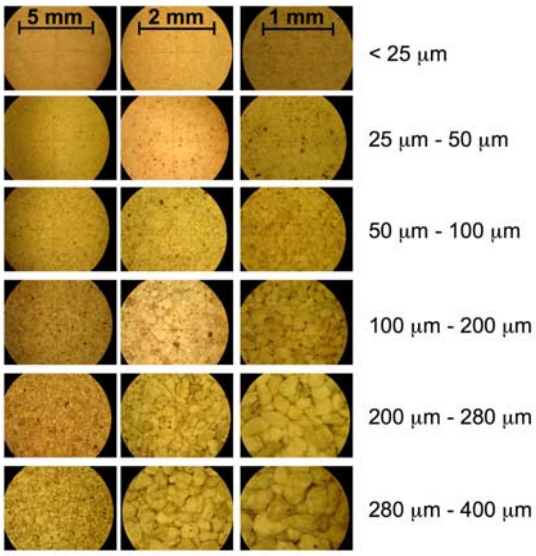

Figure 1. Pictures of six different SWy-2 smectite particle size fractions taken under a binocular microscope at three different zoom levels (zoom level increases from left to right). Large "particles" are agglomerates of much smaller particles. A small pressure applied on large agglomerates with a spatula is sufficient to divide them into very small particles which cannot be resolved under the optical microscope, even at maximum zoom level. Large particles do not present a spherical shape, but their surfaces look free from smaller particles or agglomerates at the resolution of the microscope.

[18] Altered volcanic tuff was chosen because it is a highly oxidized material that does not exhibit major spectral features in the near infrared except the strong 3-μm water of hydration absorption. The only visible crystals are millimeter-sized pyroxenes (augite). Information from the geological map of France at 1/50.000 scale, edited by the French Bureau de Recherches Géologiques et Minières (available at http://www.brgm.fr/preCarte50.do) indicates that this material was formed recently (3 Ma) during an explosive eruption caused by the interaction between magma and water. Near-infrared spectra reveal weak absorptions around 2.2 μm (Figure 5) and at 2.75 μm attributed to hydroxyls ions probably present in phyllosilicate phases. The volcanic tuff was ground by hand using a mortar and pestle and then dry sieved to separate nine fractions with different grain sizes: less than 25 μm, 25–50 μm, 50–100 μm, 100–200 μm, 200–280 μm, 280–400 μm, 400–560, 560–800 μm, and 800–1120 μm. Figure 2 presents pictures of six different particle size fractions taken on the binocular microscope at three different zoom levels. All the grains that can be resolved under the microscope present complex shapes and a coating of a very fine dust is visible on the surface of the smallest grains. This coating is so important for the three smallest grain size fractions (grains <100 μm) that individual grains are hardly resolved, even at maximum

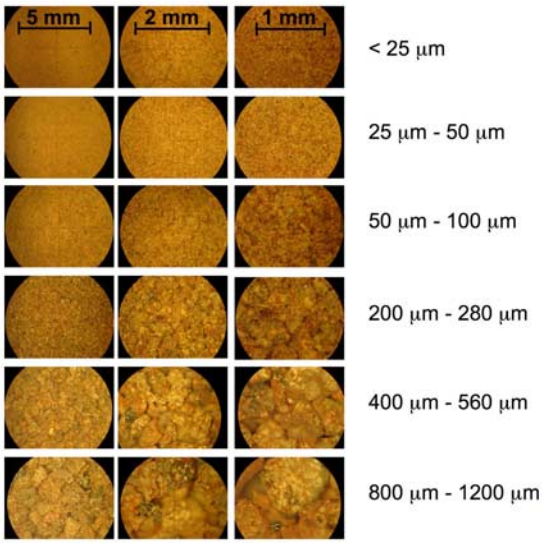

Figure 2. Pictures of six different volcanic tuff particle size fractions taken under a binocular microscope at three different zoom levels (zoom level increases from left to right). An important contamination of particles by very fine dust is observed for particle size fractions lower than 100 μm. For this reason, these particles are not resolved, even at a maximum zoom level. This contamination by very small dust is also observed but to a lesser extent for larger particles.

zoom level whereas grains in this range of diameters where resolved in the case of the SWy-2 smectite. Weaker coating (noncontiguous) is also evident for grains with sizes comprised between 100 and 280 μm and in a lesser extent for grains larger than 280 μm. We did not wash these grains to remove surface coating as other authors did, but we left this texture unchanged to observe its effect on the H_2O absorption bands.

[19] The PSOC 1532 coal is an immature coal. This material was slightly ground by hand in a mortar and pestle and then dry sieved to extract six different particle size fractions: less than 25, 25–50 μm, 50–100 μm, 100–200 μm, 200–280 μm, and 280–400 μm. Visual inspection under the binocular microscope revealed the elongated shape of all the particles, but pictures did not provide more details as the material is totally black in the visible spectral range.

[20] The majority of experiments involving mixtures were conducted with two materials chosen for their very contrasted albedo and hydration state: a smectite clay from the Clay Minerals Society Source Clay Minerals Repository (sample STx-1) and a very mature coal (anthracite) purchased from the University Coal Sample Bank and Database (sample PSOC 1468).

[21] The STx-1 smectite is a montmorillonite. Chemical composition as well as mineralogical information and physical properties are detailed by *Costanzo and Guggenheim* [2001] and Pommerol and Schmitt (submitted manuscript, 2008). The sample received from Source Clay Repository is an extremely fine powder. Contrasting with the SWy-2 smectite, no agglomerates were found. The totality of the powder passes through our finest sieve (25 μm).

[22] Anthracite is the most mature coal found on Earth. For this reason, this material is extremely dry. The most interesting property of anthracite for this study is its reflectance spectrum flatness and its strong absorption coefficient from the visible to 5 μm. Anthracite was dry sieved without grinding to produce five different grain size fractions: less than 25 μm, 25–50 μm, 50–100 μm, 100–200 μm, and 200–280 μm. Five series of samples were prepared by mixing in various proportions the STx-1 smectite powder with each anthracite grain size fraction. An illustration of these mixtures is provided on Figure 3 that presents different pictures of mixtures prepared with a constant anthracite/smectite mass mixing ratio (one-third) but different anthracite particle size fractions.

[23] We also conducted two complementary mixture experiments with two different minerals. For these experiments, anthracite was mixed in various proportions with a fine powder of gypsum (hydrated calcium sulphate, $CaSO_4 \cdot 2H_2O$; particle size <25 μm; prepared by crushing macroscopic crystals) and with the already described altered volcanic tuff 50–100 μm particle size fraction. However, unlike the previous experiment, anthracite was used unsieved.

[24] Some samples used in these experimental studies were also used in a related experimental study dedicated to highlight the effects of illumination and observation geometries variations on the hydration band strength (Pommerol and Schmitt, submitted manuscript, 2008).

2.1.1.2. Surface Preparation

[25] It is well known that the macroscopic texture of a surface has a strong effect on its reflectance spectra. To obtain a satisfactory reproducibility between the different experiments, we always used the same method to prepare the surfaces. The sample holder was filled to rim with the

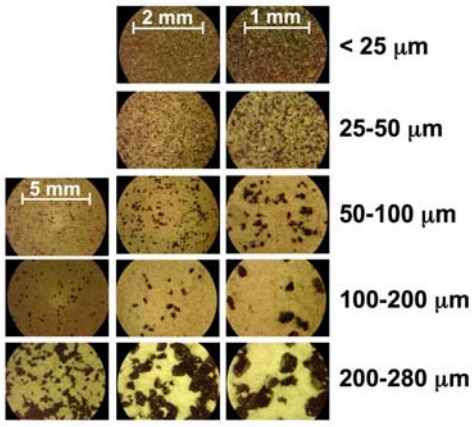

Figure 3. Pictures of anthracite and STx-1 smectite mixture samples taken under a binocular microscope at different zoom levels (zoom level increases from left to right). All the pictures were taken for a constant anthracite/smectite mass ratio of one-third. Each line corresponds to a different anthracite particle size fraction indicated on the right. Individual particles of the STx-1 smectite are extremely fine (<25 μm) and the largest aggregates are barely resolved under our optical microscope. At the resolution of our microscope, particles of anthracite always look clean from smectite on their surfaces.

Table 1. Sample Water Content Measured by Mass Loss After Heating at 300°C

Sample	SWy-2	STx-1	Volcanic Tuff	Gypsum	PSOC 1532	PSOC 1468
Mass loss at 300°C (%)	7.5	14.6	2.3	20.7	<4.8	<1.0

sample. The sample surface was then slightly packed with a tamper to obtain a flat and smooth surface at the millimeter scale. The reflectance measurements were performed on circular sample surfaces with a diameter of 3 cm and a depth varying between 1 mm and a few centimeters depending on the optical properties and the texture of the material. The sample holder depth is chosen to always obtain samples with virtually infinite optical depth at all measured wavelengths. This is easily verified by comparing measurements of the same sample with increasing depths. We considered that a sample has an infinite optical depth when no change in continuum reflectance or in contrast between continuum and absorption bands could be detected when compared with a sample of larger physical depth. Even if the same method was used to prepare all the surfaces measured in this study, the uncertainties associated with unwanted variations of surface properties (roughness, density) between samples is certainly of the order of a few percents, larger than the instrument photometric accuracy (<1%). This is probably one of the major sources of uncertainties for all the measurements presented in this paper.

2.1.1.3. Hydration State

[26] We measured the mass loss of the different types of samples when heated at a temperature of 300°C to estimate our sample water content. Approximately 300 mg of each of the samples was heated at 300°C during about 10 h. The sample mass was measured before and after heating with a precision of 0.1 mg. For each type of sample, we checked that no more mass loss occurred after longer heating times. The temperature of 300°C is probably insufficient to remove the totality of the water from our samples as shown by *Milliken and Mustard* [2005]. However, higher temperatures could dehydroxylate the samples that contain OH-ions leading to changes of sample mass not related to water content. Furthermore, thermal analyses of Clay Mineral Society source clays [*Guggenheim and Koster Van Groos*, 2001] clearly show that the large majority of the water is removed from smectites at a temperature lower than 300°C. Values of water content obtained for SWy-2 and STx-1 are in relatively good agreement with reports by *Guggenheim and Koster Van Groos* [2001]. We obtain respectively 7.5 and 14.6% of water by mass for the SWy-2 and STx-1 smectites while *Guggenheim and Koster Van Groos* [2001] obtain 7.5 and 13.3%. The value obtained for gypsum is very close to the stoechiometric value (21%). Table 1 presents results of sample water content measurements. For the two samples of coal used in this study (PSOC 1532 and PSOC 1468), it is possible that the mass loss at 300°C also includes loss of other volatiles than water, related to the decomposition of hydrocarbons. Therefore, the loss of water for these two samples at the temperature of 300°C should be considered as the maximum value corresponding to the hypothesis of a negligible decomposition of the organic matter.

[27] We investigate the effects of parameters unrelated to absolute water content on the H_2O bands of hydrated minerals. Thus, uncontrolled variations of sample water content would introduce dispersion and/or bias in the relationships obtained between band strength and particle size or albedo. For example, variations of the relative humidity in the laboratory between measurements of two different particle size fractions of the same mineral would introduce variations of water content and then band strength that are not linked to particle size. Therefore, it was necessary to ensure for the stability of sample water content during series of measurements. Then, after the measurement of each spectrum, a part of the sample (approximately 300 mg) was heated at 300°C during 20 min and its mass loss was measured with a precision of 0.1 mg.

[28] Table 2 presents the relative mass loss (difference of mass before and after heating divided by the sample mass before heating) for all particle size fractions of the three types of samples used in the first part of this study. For the montmorillonite SWy-2 and the immature coal PSOC 1532, the mass loss looks very stable for all particle size fractions indicating that no significant hydration state variation occurred during the series of measurements for these two types of samples. Furthermore, there is no evidence for a particular trend between the size of the particles and their water content for those two types of materials. Therefore, we will consider in the rest of this study that for both the montmorillonite SWy-2 and the coal PSOC 1532, all particle size fractions have the same hydration state. The case of the volcanic tuff is more problematic because relative mass loss values show a larger dispersion. However, there is no evident general trend between particle size and water content and, as shown in section 3, spectral measurements show a very strong stability of hydration band strength for all the particle size fractions larger than 100 μm. Thus, as the water content of this material is significantly lower than for the two other materials, we attribute this dispersion to measurement uncertainties rather than real variations of hydration state.

[29] Figure 4 presents the relative mass loss after heating for all the montmorillonite/anthracite and gypsum/anthracite mixtures as a function of the mixing ratio between the

Table 2. Relative Mass Loss of the Different Particle Size Fractions of Three Types of Samples After Heating at 300°C for 20 min

	Particle Size (μm)								
	<25	25–50	50–100	100–200	200–280	280–400	400–560	560–800	800–1120
SWy-2 (%)	5.2	4.8	4.9	5.2	5.4	5.2	–	–	–
PSOC 1532 (%)	3.7	3.6	3.4	3.7	3.7	3.6	–	–	–
Volcanic tuff (%)	1.9	2.1	1.7	1.5	1.3	1.4	1.1	1.2	1.9

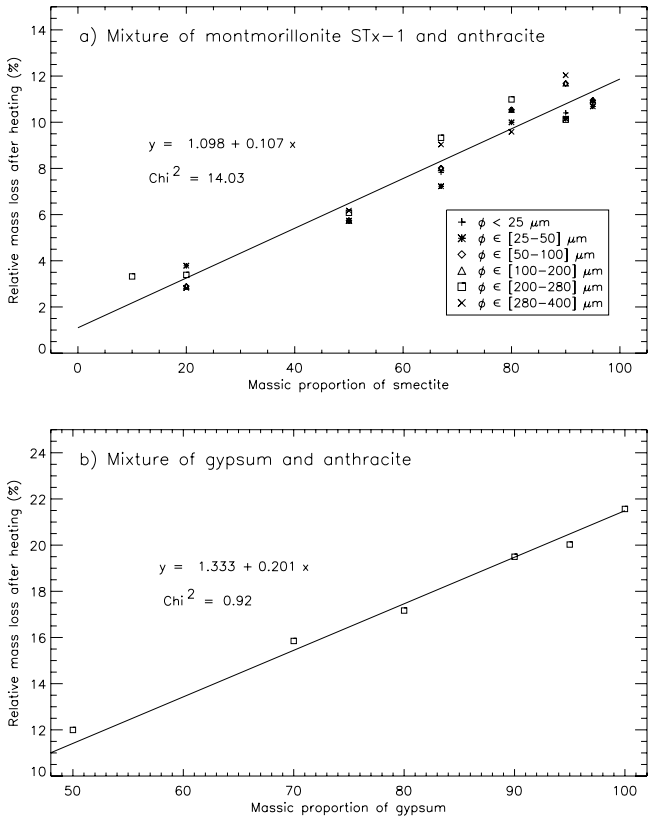

Figure 4. Relationship between mass loss on heating at 300°C and mixing ratio for the (a) montmorillonite/anthracite mixtures and (b) gypsum/anthracite mixtures. Straight lines are the best fit lines between mass loss and mixing ratio. Equations and chi^2 values for these linear fits are provided on each plot.

hydrated mineral and the relatively dry anthracite. Superposed to the measurements, we plot the best fit lines. Low values of χ^2 associated with these two fits confirm that sample water content is proportional to the mixing ratio between the hydrated and the dry material. Unfortunately, the low water content of the volcanic tuff/anthracite mixture (<2%) does not permit an accurate measurement of water content for these samples. However, all measurements for these mixtures were performed within the same day and with a constant temperature in the room. We can then reasonably assume that as for the other mixture samples, sample water content was only controlled by the mixing ratio between the two components.

2.1.2. Reflectance Measurements

[30] Reflectance spectra were measured with the LPG Spectrogonio radiometer [*Brissaud et al.*, 2004]. This instrument is designed to measure reflectance spectra of particulate sample surfaces in the visible and near-infrared spectral ranges (0.3–4.8 μm) with a high degree of radiometric accuracy over wide angular ranges. All the measurements presented in this paper cover the 1.0–4.2 μm range that includes the 1.9- and 3-μm H_2O bands and were recorded in a "standard" low phase angle geometry (incidence = 0°, emergence = 30°). The incident beam illuminates the totality of the sample surface and the area observed by the detector is an ellipse that is 2.3 × 2 cm wide. As the sample holder itself is circular with a diameter of 3 cm, we can consider that the part of the sample observed by the detector is always representative of the bulk composition of the sample. All measurements have been performed under ambient conditions in a laboratory equipped with air conditioning (temperature: 25 ± 1°C). We have chosen a constant spectral sampling of 0.02 μm, of the same order of magnitude as the majority of the near-infrared imaging spectrometers collecting data on planetary surfaces.

[31] Calibration of the sample reflectance spectra is performed by dividing the raw spectrum of the sample by the spectrum of reference surfaces. The reference surfaces used are Spectralon© (Labsphere Inc.) for the 0.4–2.5 μm spectral range and Infragold® (Labsphere Inc.) for the 2.5–4.8 μm spectral range. Several corrections are applied to calibrate the reflectance spectra with an absolute photometric accuracy better than 1% at all wavelengths and all geometrical configurations. This includes corrections of the reference reflectance spectra based on Labsphere spectral data and on our own absolute bidirectional reflectance distribution function (BRDF) calibrations. Corrections of some instrumental artifacts are also taken into account (see *Bonnefoy* [2001] for more details on the calibration procedure).

2.2. Radiative Transfer Numerical Modeling

2.2.1. Radiative Transfer Model

[32] We use the bidirectional reflectance model developed by *Douté and Schmitt* [1998] that calculates the radiative transfer of solar light through a dense granular medium. This model, based on *Chandrasekhar*'s [1960] theory, can be considered as an improvement of the widely used *Hapke*'s [1993] model. Significant differences exist between these two models (see the detailed discussion by *Douté and Schmitt* [1998]). However, for a semi-infinite medium, all differences appear in the calculation of the multiple scattering terms in the case of anisotropic scattering by the granular medium. In this study, we always assume that scattering by particles is isotropic. In these conditions, the model we used can be considered strictly similar to Hapke's model.

[33] The entries of the model are a set of free parameters that describe the surface physical properties (grain size, mixing ratios, etc.) and the observation geometry (incidence, emergence, and azimuth angles). The model also requires the intrinsic optical indices (n, k) of the materials (see section 2.2.2). We build libraries of synthetic spectra by varying by steps the different free parameters (particle size, mixing ratio) to match as much as possible the parameters used in physical laboratory experiments. In this paper the incidence and emergence angles are fixed to 0° and 30° respectively. The effects of these geometry parameters are studied in detail in an upcoming paper (Pommerol and Schmitt, submitted manuscript, 2008). The synthetic spectral libraries are calculated with a spectral sampling and a spectral resolution similar to the measured spectra (~0.02 μm).

[34] As the radiative transfer model is based on geometric optics physical laws, spectra of materials with very fine grains cannot be modeled. The longest wavelength used to calculate the 3-μm band strength being around 4 μm, we never calculate spectra with a particle size lower than 10 μm in order to keep the "optical size parameter," $x = \pi.D/\lambda$ (where D is the particle diameter and λ the wavelength) in the valid range of geometrical optics.

2.2.2. Optical Constants

[35] The radiative transfer model we use requires the knowledge of the material's intrinsic optical constants (complex indices n and k). The determination of optical indices from laboratory measured spectra is highly challenging. Therefore, we did not try to determine the optical constants of our samples directly from our own laboratory measurements but decided to use the optical constants of the SWy-1 smectite (Clay Mineral Society) published by *Roush* [2005]. This author proposes a new method to extract optical constants from laboratory measured reflectance spectra relying on a combination of scattering theory and Kramers-Kronig analysis. The main improvement of this method is the determination of wavelength dependent real indices. This is a very important point as the real index (or refraction index n) is known to show large variations around strong fundamental absorption bands. As this is the case for the 3-μm band, it is crucial to use optical constants that correctly take this property into account. The mineral used by *Roush* [2005] (SWy-1 smectite) is almost the same than one of the materials we use in our laboratory measurements (SWy-2 smectite). These materials distributed by the Clay Mineral Society have the same origin and chemical and mineralogical properties. The only difference between the SWy-1 and SWy-2 smectites is the time at which they were collected.

[36] To simulate physical experiments involving mixtures between a hydrated smectite and anthracite, we calculated a synthetic optical constant set designed to simulate the almost totally flat spectra of anthracite with very low reflectance for all particle sizes (see Figure 9). This was done by fixing the real index (n) and the absorption coefficient (α) at constant values over the whole spectral range (n = 2 and α = 1300 cm^{-1}) and then calculating the wavelength dependant imaginary part of the complex index k(λ). These values of n and α were chosen according to the experimental study and discussion by *Manickavasagam and Menguc* [1993].

[37] In physical experiments, STx-1 smectite was used as the high-albedo hydrated component instead of the SWy-1 smectite. However, optical constants for this smectite have not been measured over the spectral range relevant for this study. Therefore, we compare these physical experiments with simulated granular mixtures of the SWy-1 smectite and the synthetic dark component described above. The main difference between the STx-1 and SWy-1 smectites in their spectral properties is related to their water content (STx-1 being more hydrated that SWy-1, see Table 1). This discrepancy will not allow for direct comparisons between absolute values derived from experiments and modeling but should not modify the general trends as a function of mixing ratio and particle size.

2.3. Rationale for the Comparisons Between Measurements and Modeling

[38] As detailed in this section, both experimental and modeling approaches are used in this study. However, our objective is not to provide direct comparisons between results from experiments and modeling. Physical experiments and radiative transfer modeling are applied on different types of materials that differ by their chemistry, texture, and water content. These differences between the materials often prevent from direct comparisons between the absolute values of spectral criteria calculated from measured or calculated spectra. Only the relative trends between studied parameters, particle size, albedo, and band strength, can be compared. Therefore, we never tried to fit any of the results from physical experiments by numerical simulations.

[39] The objective of comparing measurements and modeling in this study is to obtain robust conclusions about the effects simultaneously observed on real samples in the laboratory and quantitatively described by the physical theory of radiative transfer. Robustness comes from the complementary advantages and weaknesses of these two different approaches. On one hand, laboratory experiments offer the ground truth that is often inaccessible on planetary surfaces and represent all the complexity of natural surfaces. On the other hand, it is always difficult to perfectly control all experimental conditions, especially when working with very volatile species like water. Radiative transfer modeling only offers approximations in all the relationships between the different parameters. However, the individual effects of all the parameters can be easily separated and studied.

2.4. Definition of Hydration Band Spectral Criteria

[40] We calculate different spectral criteria to estimate the strength of the absorptions at 1.9 and 3 μm and to compare their behaviors at constant hydration level under the effects of changes in grain size and albedo. The most common of these spectral criteria is the band depth defined by *Clark and Roush* [1984] as

$$\mathrm{NBD}(\lambda) = 1 - \frac{\mathrm{R}(\lambda)}{\mathrm{R_c}(\lambda)}$$

where R(λ) is the reflectance at the wavelength λ (usually the maximum of absorption) and $R_c(\lambda)$ is the value of a continuum defined above the absorption band at the same wavelength. This definition corresponds, in fact, to a normalized band depth (relative to the continuum) and is hereinafter referred to as "NBD". Another definition of band depth was proposed by *Morris et al.* [1982] as a simple difference of reflectance between the band and the continuum: $BD(\lambda) = R(\lambda) - R_c(\lambda)$. In this definition, no normalization is implied. Then, this spectral criterion will be hereinafter referred to as "BD".

[41] Figure 5 presents an illustration of band depth calculation for the 1.9- and 3-μm bands. BD and NBD are also calculated at different wavelengths for the 3-μm band. The maximum of absorption for the 3-μm band is located around 2.9 μm. However, as absorption is saturated at this wavelength for a number of our samples, in addition to values at 3.0 μm we also calculated BD and NBD at 3.2 and 3.4 μm. As the 3-μm hydration absorption band covers a large wavelength range, we also use integration criteria to estimate the strength of this band. The integrated band depth (IBD) is the band depth criterion described above that is discretely integrated for each wavelength on a predefined spectral range. We made the choice to integrate the 3-μm band between 2.9 and 3.8 μm to avoid absorption due to hydroxyl ions around 2.7 μm. On the long-wavelength wing of the 3-μm band, 3.8 μm is the wavelength where reflectance is maximal on the majority of our samples. We

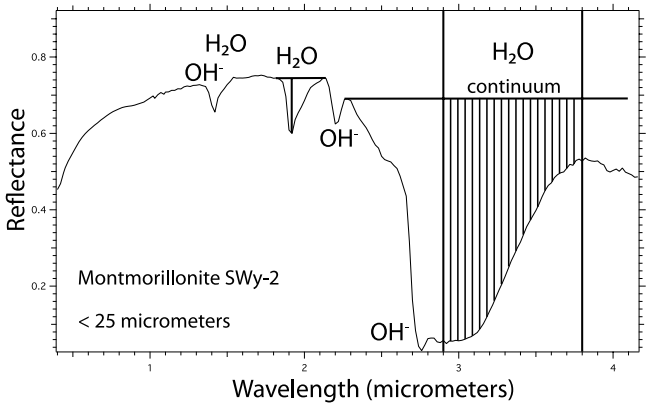

Figure 5. Laboratory measured spectrum of the SWy-2 smectite with particle size smaller than 25 μm. This plot shows the attributions of the different absorption bands due to H_2O and OH- and illustrates some of the spectral criteria used to estimate the strength of the 1.9- and 3-μm H_2O absorption bands. See text for the definitions of these spectral criteria.

also calculated the integrated band area (IBA) obtained by discrete integration of the difference between the continuum and the spectrum reflectance (BD) at each wavelength. IBA can then be normalized by the continuum reflectance to obtain the normalized integrated band area (NIBA). For all these criteria it is necessary to define a continuum above the absorption band to integrate its intensity. We have chosen to follow the definition of a flat continuum with a constant value as recommended by *Milliken and Mustard* [2007a]. We tested different values for this continuum: the maximum of reflectance between 1 and 3 μm [*Milliken and Mustard*, 2007a], the last local maximum in the continuum before the 3-μm absorption band (around 2.3 μm) or other points between 1 and 2.3 μm. However, if absolute values of the spectral criteria can vary by a few percent according to the continuum definitions, we always obtain very similar results in terms of general relative trends when using these different values. Therefore, we only present values calculated with a flat continuum equal to the value of the local reflectance maximum, around 2.3 μm, before the 3-μm absorption band (Figure 4). It must be noted that there is a very small absorption by water at this wavelength. This is not problematic in this study because absorption is negligible compared to the 3-μm region but a definition of the continuum at 2.15 μm instead of 2.3 μm would be more appropriate for samples with lower water contents. This definition avoids taking into account an eventual slope in the near-infrared spectrum continuum that would not be linked with mineral hydration [*Fischer and Pieters*, 1993]. It also makes the NIBA and IBD criteria similar in their formulations. Results for the NIBA criterion can then be directly compared with IBD values presented by other authors [*Calvin*, 1997; *Jouglet et al.*, 2007].

[42] The same criteria were also calculated from spectra converted from reflectance to apparent absorbance ($-\ln(R)$) and to single-scattering albedo using equation 11.6 from *Hapke* [1993]. In this last case, we also calculated the ESPAT criterion from the single-scattering albedo spectra using the formula proposed by *Milliken and Mustard* [2007a].

3. Results

3.1. Pure Materials With Variable Particle Size

3.1.1. Reflectance Spectra

[43] The reflectance spectra of the four materials used in this part of the study are presented in Figure 6. Three series of experimental spectra (SWy-2 smectite, volcanic tuff, and coal PSOC 1532) have been measured for all separated particle size fractions. A series of modeled spectra of SWy-1 smectite is also presented with particle sizes corresponding to the average sizes of the SWy-2 fractions (rounded values were used) to allow a direct comparison.

[44] These four series of measured and modeled spectra all show the well-known effect of increasing the continuum reflectance level when decreasing the average particle size. We can note that the effect of particle size variation on the continuum reflectance level is stronger on the modeled spectra of the SWy-1 smectite (Figure 6b) than on the measured spectra of the SWy-2 smectite (Figure 6a). A speculative but plausible hypothesis to explain this discrepancy is the aggregated nature of the SWy-2 "grains" that can lead to an effective particle size that is different in terms of radiative transfer than the one obtained by sieving. The presence of a very thin coating of very small dust grains on the large particles also cannot be rejected.

[45] The evolution of the volcanic tuff reflectance spectra with particle size (Figure 6c) shows an important gap between the spectrum of the 100–200 μm fraction and the spectra of the three finest fractions. Furthermore, differences between the spectra of the three smallest grain size fractions are extremely small, which strongly departs from the evolution of the modeled and measured spectra of the SWy-1 and SWy-2 smectites (Figures 6a and 6b). We attribute this effect to the coating of very fine dust present on larger grains that was revealed by inspection under the microscope (Figure 2). The spectra are in good agreement with microscopic observations as the three finest particle size fractions appeared to be much more contaminated by dust than all the other fractions. These very fine dust coatings apparently control the optical behavior of these three samples.

[46] At wavelengths shorter than 2.7 μm the relative variations of reflectance as a function of particle size are particularly strong for the coal PSOC 1532 (Figure 6d). The strong absorption at wavelengths longer than 2.7 μm is totally saturated for all particle size fractions except the smallest one. However, we cannot use this 3-μm band in this study as C–H modes of hydrocarbons present in this immature coal are probably the major contributor to this band, hiding the H_2O absorption. Therefore, we only study the 1.9-μm hydration band of this material.

3.1.2. Quantitative Effect of Particle Size on the Hydration Bands

3.1.2.1. 3-μm Hydration Band

[47] Figure 7 presents the quantitative effect of grain size variations on the 3-μm hydration band estimated with the different spectral criteria previously defined. NBD calculated at 3.0 and 3.2 μm from the reflectance spectra of the 3 studied materials shows very similar evolutions as a function of

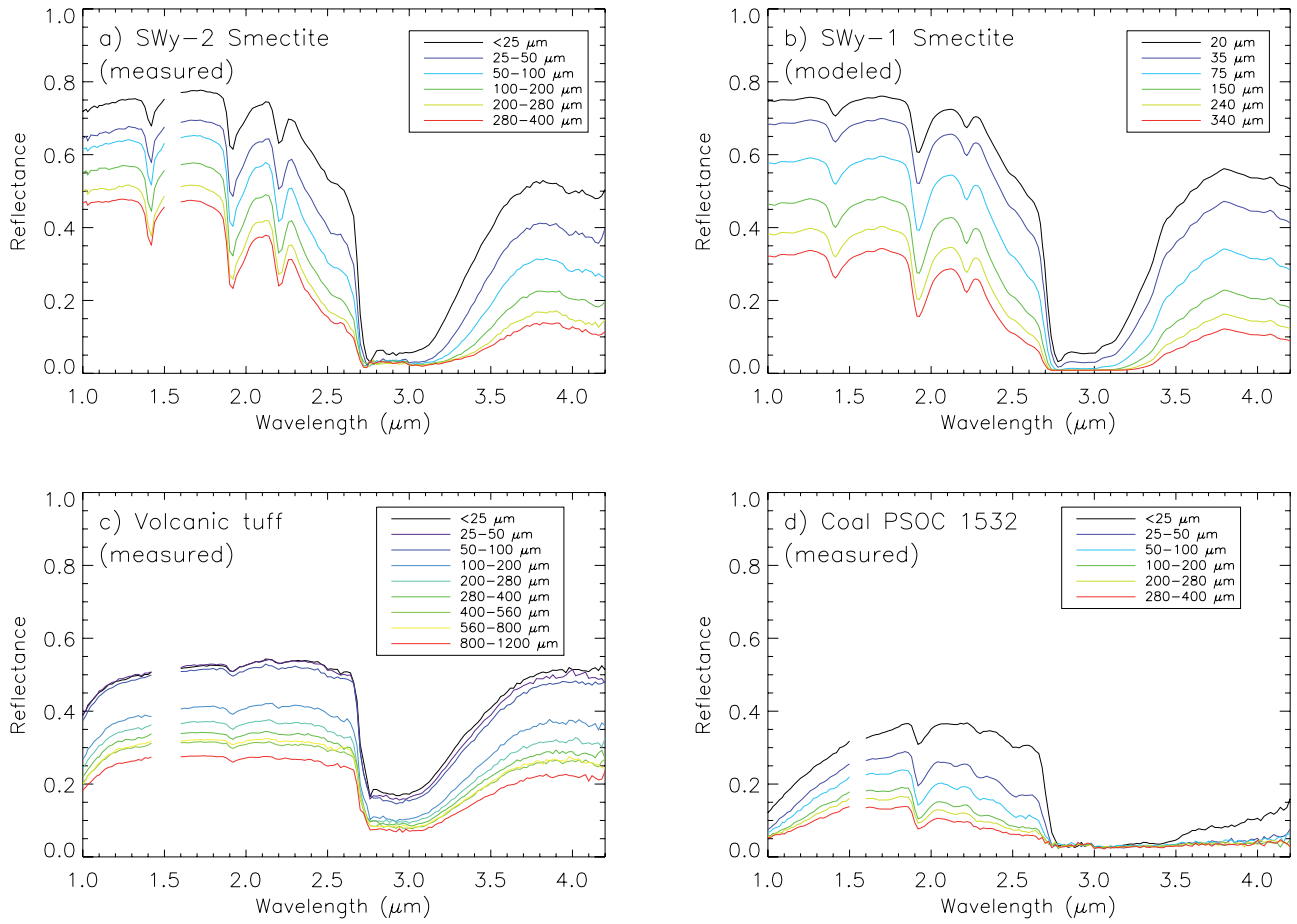

Figure 6. Pure materials. Series of near-infrared reflectance spectra of four different materials with varying particle size. Measured spectra: (a) SWy-2 smectite, (c) volcanic tuff, (d) coal PSOC 1532. (b) Modeled spectra: SWy-1 smectite. All plots show the same first-order effect: a general increase of reflectance when particle size decreases.

particle size (Figure 7a). Normalized band depth is almost constant for the largest particle size fractions but decreases with decreasing particle size for the smallest fractions (<50–100 μm). In the case of smectites (modeled SWy-1 and measured SWy-2), this evolution depicts the desaturation of the 3-μm hydration band occurring below a threshold particle size (Figure 6). This "threshold particle size" depends on the wavelength at which band depth is calculated. Even when the 3-μm absorption band is not saturated with the largest grain sizes, as for the volcanic tuff spectra, the same evolution of the 3.0 and 3.2 μm normalized band depth parameters is observed: no significant variation for particle sizes larger than 150 μm but a clear decrease below 100 μm. In that case, this behavior cannot be attributed to the desaturation of the absorption band but rather to a change in the relative evolution of the band and continuum reflectance values. This corresponds to the transition from surface-to volume-dominated scattering processes. We can again notice a significant difference between the values obtained for the three smallest particle size fractions and the 100–200 μm fraction. This discontinuity, first revealed on reflectance spectra (Figure 6), is due to the dominant effect of the very fine dust coating the smallest grains. However, the size variation of the underlying grains has still a noticeable effect on the band depth.

[48] NIBA calculated from reflectance spectra (Figure 7b) shows a relatively similar dependence to particle size than NBD, except its sensitivity to small particle sizes that is stronger and extends to somewhat larger sizes. Good consistency is observed between the experimental results for the SWy-2 smectite and the radiative transfer modeling (SWy-1 smectite) in the range of particle sizes where both methods were applied. It must be noted that no scaling has been applied for comparison. The same absolute values obtained for both the measured (SWy-2) and modeled (SWy-1) smectites denote a very similar hydration state of these two materials during measurements. At first order, NIBA calculated from the volcanic tuff reflectance spectra and from the smectite reflectance spectra present similar dependencies on particle size. Minor discrepancies for the smallest grain size are attributed to the coating of fine grains on the larger ones.

[49] In order to study how the above size-dependent behaviors are affected, the normalized band depth and normalized integrated band area were also calculated after conversion of the reflectance spectra to single-scattering albedo spectra. As can be seen on Figures 7c and 7d, conversion to single-scattering albedo does not change the global shape of the relationship between the 3-μm band

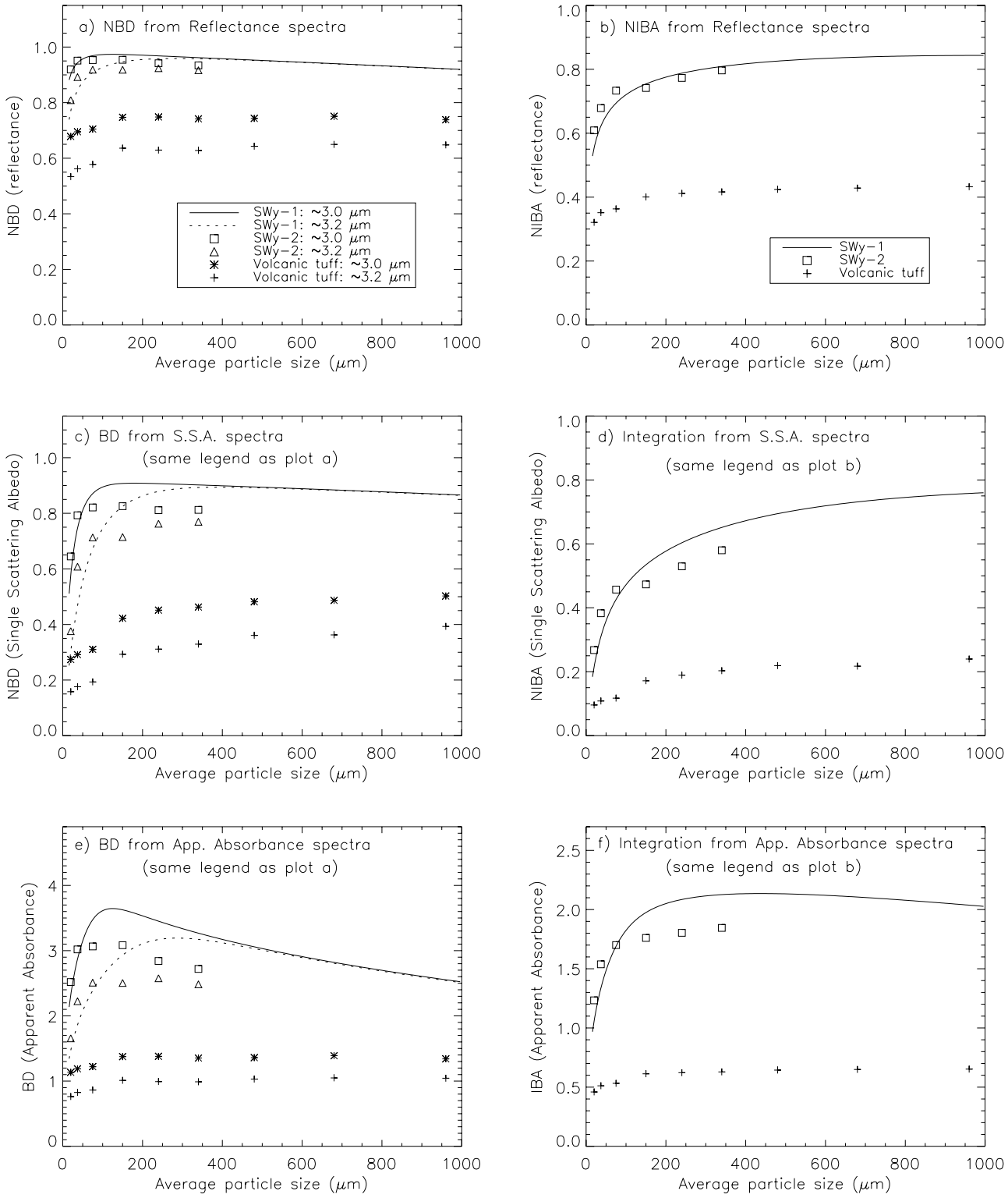

Figure 7. Pure materials. Evolution of the 3-μm band strength criteria as a function of material particle size. In each plot, the band strength is calculated with a different spectral criterion (see text for definitions). (a, c, and e) Criteria calculated at two discrete wavelengths (2.9 and 3.2 μm). (b, d, and f) Integrated spectral criteria (between 2.9 and 3.8 μm). These criteria are calculated from experimental spectra recorded for two materials (SWy-2 smectite and volcanic tuff) and on synthetic spectra (SWy-1 smectite).

strength estimation criteria and particle size but strongly increases (by factors 2.5 to 4) the influence of particle size on the NIBA criterion and only for the smallest size fractions on NBD. In addition, significant variations of NBD and NIBA occur for medium and large particles in the case of unsaturated 3-μm bands (volcanic tuff), whereas these criteria were not sensitive to these particle sizes when expressed in reflectance. For example, in the case of the volcanic tuff, relative increase of NIBA between the particle size fractions 100–200 μm and 800–1120 μm is 7% when NIBA is calculated from reflectance spectra and 30% when NIBA is calculated from single-scattering albedo spectra. Conversion to single-scattering albedo is thus not a solution to reduce the grain size effect on any water content estimation criteria.

[50] Finally, when converted to apparent absorbance, the relationships between the 3-μm band strength criteria and particle size have quite different behaviors for the smallest particle size fractions (Figures 7e and 7f). For saturated 3-μm bands (measured and modeled smectites), the normalized band depths at 3.0 and 3.2 μm display a maximum at one particular particle size (dependant on wavelength) and markedly decrease for particle sizes larger than this particular value. On the other side, the IBA parameter, while strongly sensitive at small particle sizes (<200 μm), displays only limited variations for larger sizes. For the volcanic tuff no such behaviors are observed. The relative variations of band strength (NBD and IBA) for this material are very similar to what is obtained with reflectance spectra (Figures 7a and 7b). The origin of this difference in behaviors between smectites and volcanic tuff is linked to the difference in their water content and thus to the absolute value of their 3-μm band strength (saturated versus unsaturated bands). Conversion of reflectance to apparent absorbance has a differential effect only for low values of reflectance (near-saturated bands or low-albedo materials) but has no effect on hydration bands that are far from saturation (as for the 1.9-μm band, see section 3.1.2.2).

3.1.2.2. 1.9-μm Hydration Band

[51] The evolutions of the 1.9-μm band strength, estimated with different criteria, as a function of particle size are presented in Figure 8. Criteria using integration have been also calculated and compared to the simple BD and NBD criteria. However, in the case of the 1.9-μm band, they present the same evolutions and relative variations than NBD, contrasting to what was observed for the 3-μm band. Therefore, we only present the results obtained for NBD, as this criterion is generally used to characterize the spatial variations of this band on solar system surfaces. The 1.9-μm hydration band being too weak in the reflectance spectra of volcanic tuff to study its evolution with particle size; we focus this study on the SWy-2 and SWy-1 smectites (measured and modeled, respectively) and on the coal PSOC 1532.

[52] When calculated from reflectance spectra, the NBD at 1.9 μm shows very strong dependences on particle size (Figure 8a). For the SWy-2 smectite it increases by a factor 2.5 from the less than 25 μm fraction to the 280–400 μm fraction. As already noted for the 3-μm band, the consistency between measurements (SWy-2 smectite) and modeling (SWy-1 smectite) is good. *Cooper and Mustard* [1999] also measured the 1.9-μm NBD from laboratory spectra of SWy-1 smectite but for very fine particle sizes ranging between 2.5 and 50 μm. These data show a steep decrease of NBD for decreasing particle sizes, consistent with our measurements (Figure 8a). Taken together, these two sets of experimental data show the extremely strong sensitivity of the 1.9-μm water of hydration band strength with particle size and thus the crucial influence of surface texture on the detection limit of this band in planetary observations.

[53] For the PSOC 1532 coal, the evolution of NBD at 1.9 μm appears similar to the one of smectites for the smallest particle size fractions but is quite different for larger particles (>200 μm) where NBD remains at an almost constant value for the coal whereas NBD continues to increase for smectites. The main difference between smectites and coal spectra is the value of the reflectance in the continuum: low for the PSOC 1532 coal and high for smectites (Figures 6a and 6d). For this reason, the transition from volume to surface scattering occurs at a smaller particle size for the coal than for the smectite.

[54] Conversion of reflectance to apparent absorbance does not change at all the relationship between band strength and particle size. The same conclusion has been already drawn for the 3-μm band in the case of the volcanic tuff. Conversion to apparent absorbance has only an effect on absorption bands close to saturation. When bands are close to saturation, conversion to apparent absorbance seems to increase the effects of particle size variations.

[55] Conversion of reflectance to single-scattering albedo leads to larger relative variations of NBD with particle sizes compared to the one calculated from reflectance spectra (Figure 8c). The ESPAT parameter calculated from single-scattering albedo spectra shows the same evolution than NBD. Conversion to single-scattering albedo also considerably deteriorates the agreement between results from physical experiments and physical modeling. This is due to the strong nonlinearity of the relationship between reflectance and single-scattering albedo and to the assumptions (scattering phase function, etc.) needed for this conversion that obviously induce accuracy problems which propagate in the extraction of parameters from single-scattering albedo spectra (see Figure 8 and discussion by *Milliken and Mustard* [2005]).

3.2. Mixtures Between Hydrated Material and Dark Material With Variable Particle Size

3.2.1. Reflectance Spectra

[56] Five series of reflectance spectra of granular mixtures between STx-1 smectite (particle size <25 μm) and a dark and relatively dry component (anthracite) have been measured for this study of the effects of mixing and albedo on the 1.9- and 3-μm hydration band strengths. Each series corresponds to a different grain size fraction of anthracite mixed in variable amounts with smectite (Figure 3). The pure components have been also measured. The series with the smallest and largest anthracite particle sizes (less than 25 μm and 200–280 μm, respectively) and with an intermediate size (50–100 μm) are presented on Figure 9 associated with the corresponding series of modeled spectra.

[57] The two other series of measurements with intermediate anthracite particle sizes (25–50 μm and 100–280 μm), not presented here, as well as the modeled spectra show the same global effects, i.e., a strong decrease of continuum

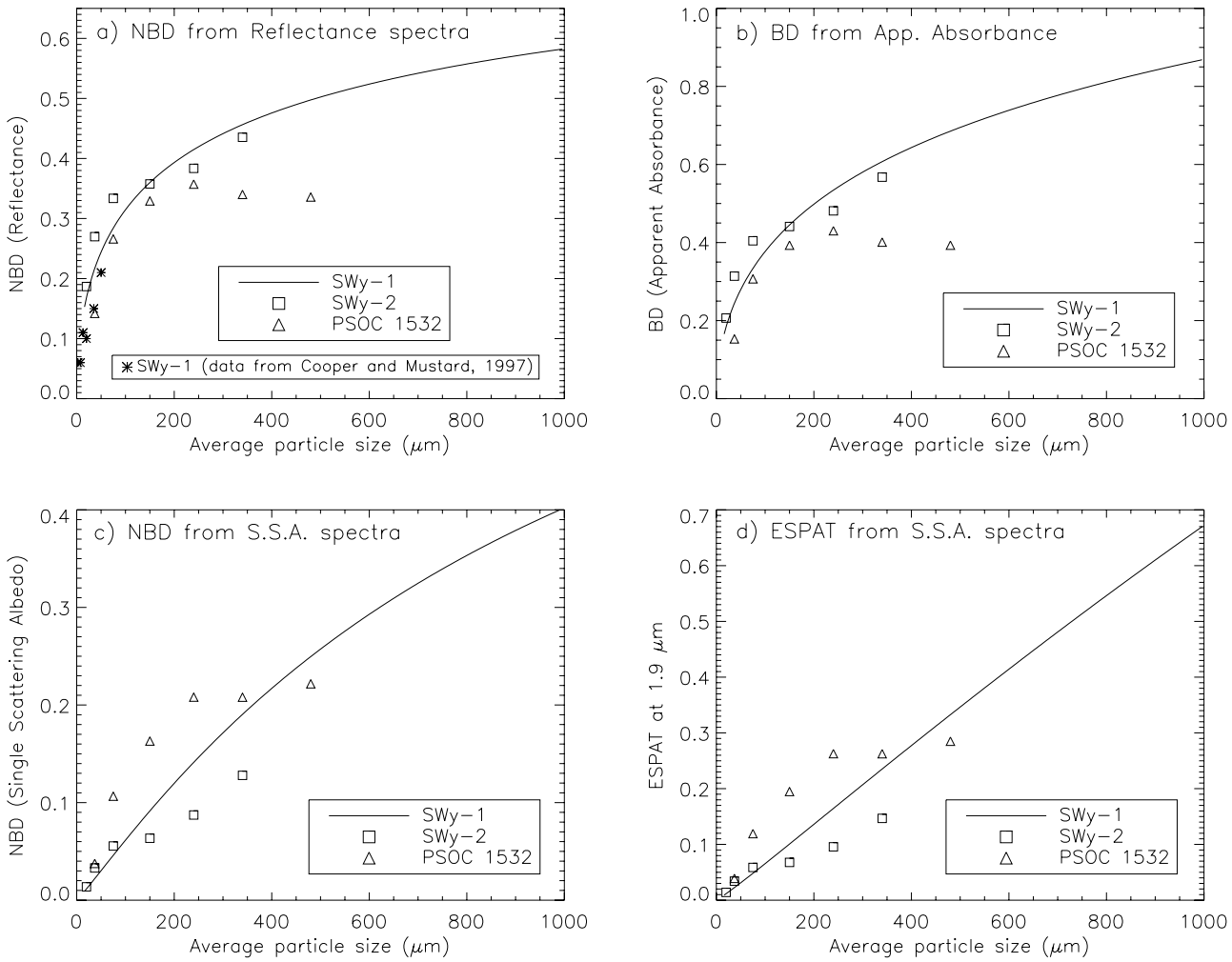

Figure 8. Pure materials. Evolution of the 1.9-μm band strength as a function of material particle size. In each plot, the band strength is calculated with a different spectral criterion (see text for definitions). These criteria are calculated from experimental spectra recorded for two materials (SWy-2 smectite and coal PSOC 1532) and on synthetic spectra (SWy-1 smectite). On Figure 8a we added the experimental data from *Cooper and Mustard* [1999] for very fine particles of SWy-1 smectite.

reflectance and band depth as a function of the amount of anthracite in the mixture. This behavior appears highly dependent on the anthracite particle size. With the smallest anthracite particle size fraction, reflectance decreases drastically with small amounts of this very dark material. For larger particle sizes, larger amounts of anthracite are needed to lower the reflectance of the mixture by the same amount. The same kind of effects can be expected for the absorption band strengths.

[58] Absolute reflectance values of the pure dark material are notably inconsistent between the measured and modeled data sets. In measured spectra, pure anthracite shows relatively high values of reflectance that tend to increase with wavelength and particle size (up to 10% of reflectance at 4 μm for the largest particle size). These effects are not reproduced at all by radiative transfer modeling using constant values of n and α. We have run the model with different values of the optical constants but the effects observed on the measured spectra appear impossible to reproduce. A plausible hypothesis to explain the behavior of anthracite reflectance in measured spectra is a partial orientation of the coal particles (carbon sheets) during sample surface preparation. This would produce a small amount of specular reflections on smooth particle faces that could explain the high values of reflectance and that is not taken into account in the model (isotropic particles).

3.2.2. Quantitative Effects of Mixtures on the Hydration Bands

3.2.2.1. 3-μm Hydration Band

[59] Figure 10 presents the evolutions of NBD at 3.4 μm (the absorption band is totally saturated at 3.0 and 3.2 μm), IBA, and NIBA calculated from reflectance spectra as a function of the amount of anthracite for the five experimental series of mixtures (Figures 10a, 10c, and 10e) and for the corresponding series of modeled spectra (Figures 10b, 10d, and 10f). The average particle size of the corresponding fractions is used in the models (rounded values are used), except for the finest fraction where we run two models with 10- and 20-μm diameter particles. The water content of the mixtures is proportional to the amount of smectite in these mixtures and thus varies linearly with the proportion of anthracite. This was verified by measuring the mass loss

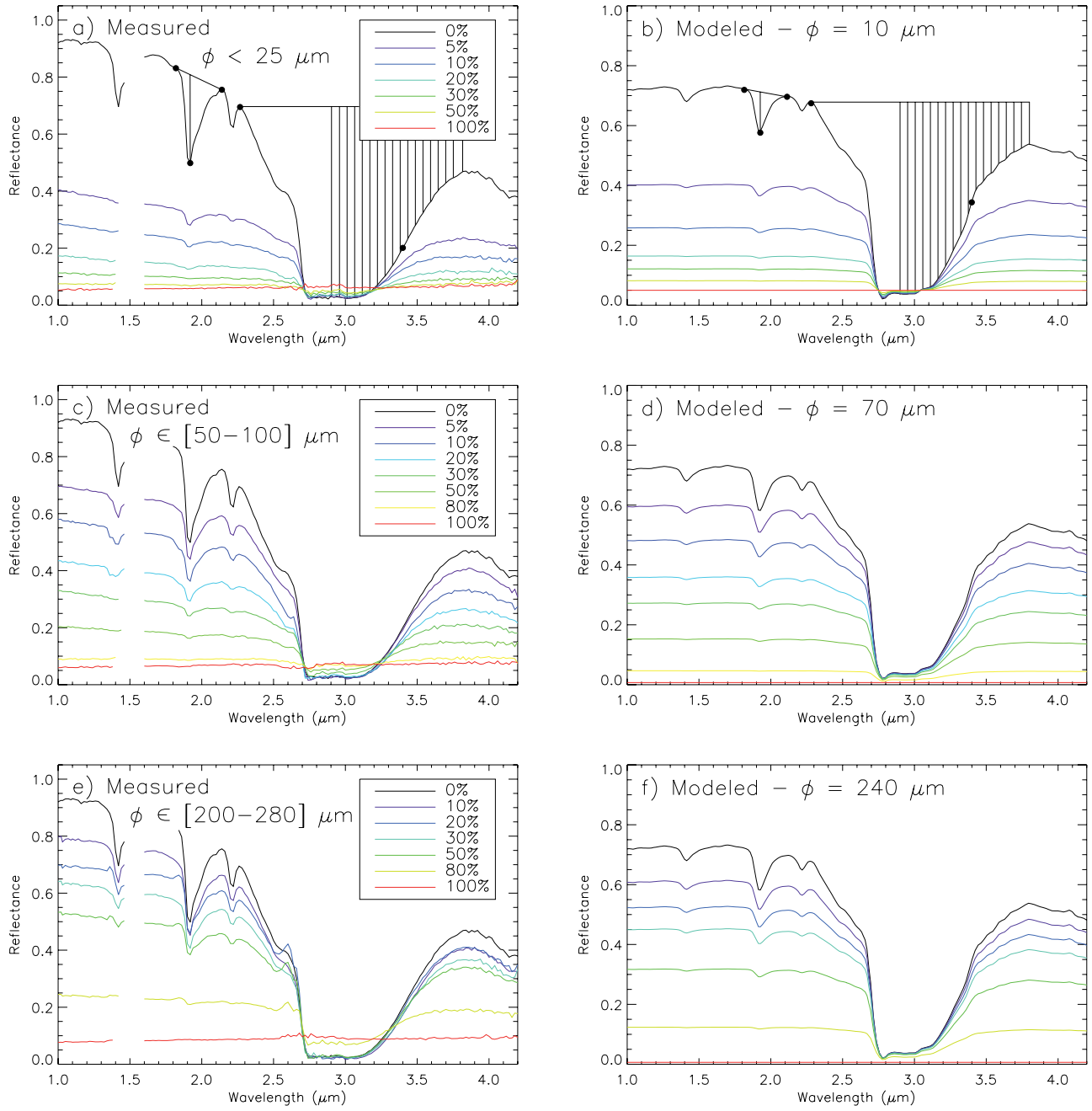

Figure 9. Series of near-infrared reflectance spectra of granular mixtures between smectite powder and a dark material. (a, c, and e) Measurements using STx-1 smectite (particle size <25 μm) and anthracite as the dark material. (b, d, and f) Modeling using SWy-1 smectite and a synthetic dark component. Each row corresponds to a different particle size of the dark material in the mixture. The model uses an estimated mean particle size. The amounts of dark component in the mixtures are expressed in mass percentage. Reflectance and band strength decrease with increasing proportions of the dark component but at a rate highly dependant on the dark particle size. We superpose illustrations of the methods used to calculate different hydration band strength spectral criteria to the spectra of smectites in Figure 9a and 9b.

after heating at 300°C for all the prepared mixtures. The quantitative relationship between mixing ratio and water content is presented on Figure 4.

[60] The plots on Figure 10 clearly show that for a same amount of dark material, the strength of the 3-μm band strongly depends on the particle size of the dark material introduced in the mixture. Normalization of the IBA by the reflectance in the continuum changes the shape of this dependence but does not remove or even reduce it (Figures 10e and 10f).

[61] The agreement between the results from physical experiments and numerical radiative transfer modeling is globally good. The relative variations of the various band strength criteria with particle sizes are well reproduced even

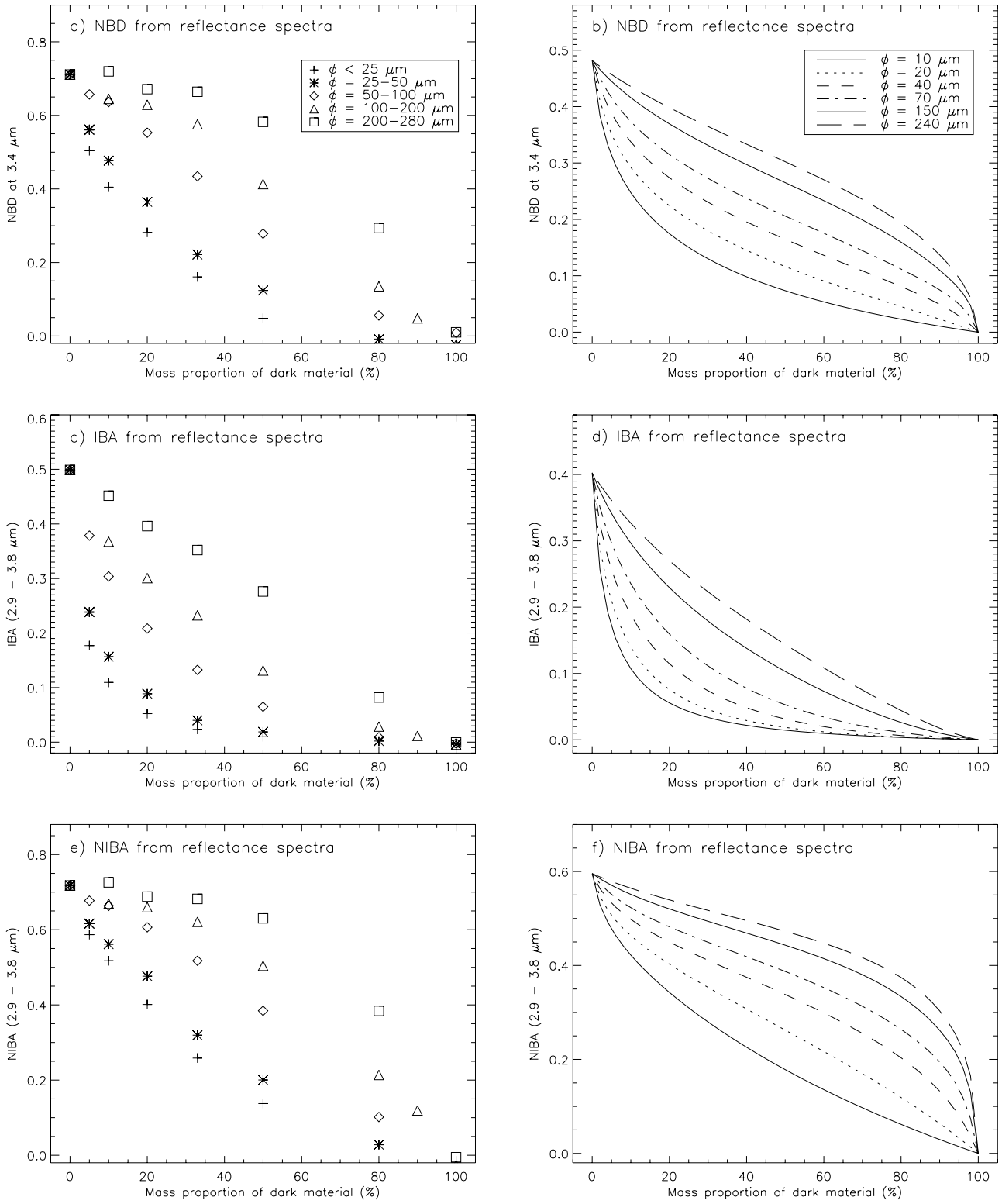

Figure 10. Granular mixtures. Evolution of the 3-μm absorption band strength criteria (normalized band depth (NBD), integrated band area (IBA), and normalized integrated band area (NIBA)) as a function of dark material/smectite mixing ratio for different particle sizes of the dark component. All these criteria are calculated from reflectance spectra. (a, c, and e) Experimental results (mixture of STx-1 smectite and anthracite PSOC 1468). (b, d, and f) Radiative transfer modeling (mixture of SWy-1 smectite and a synthetic dark material).

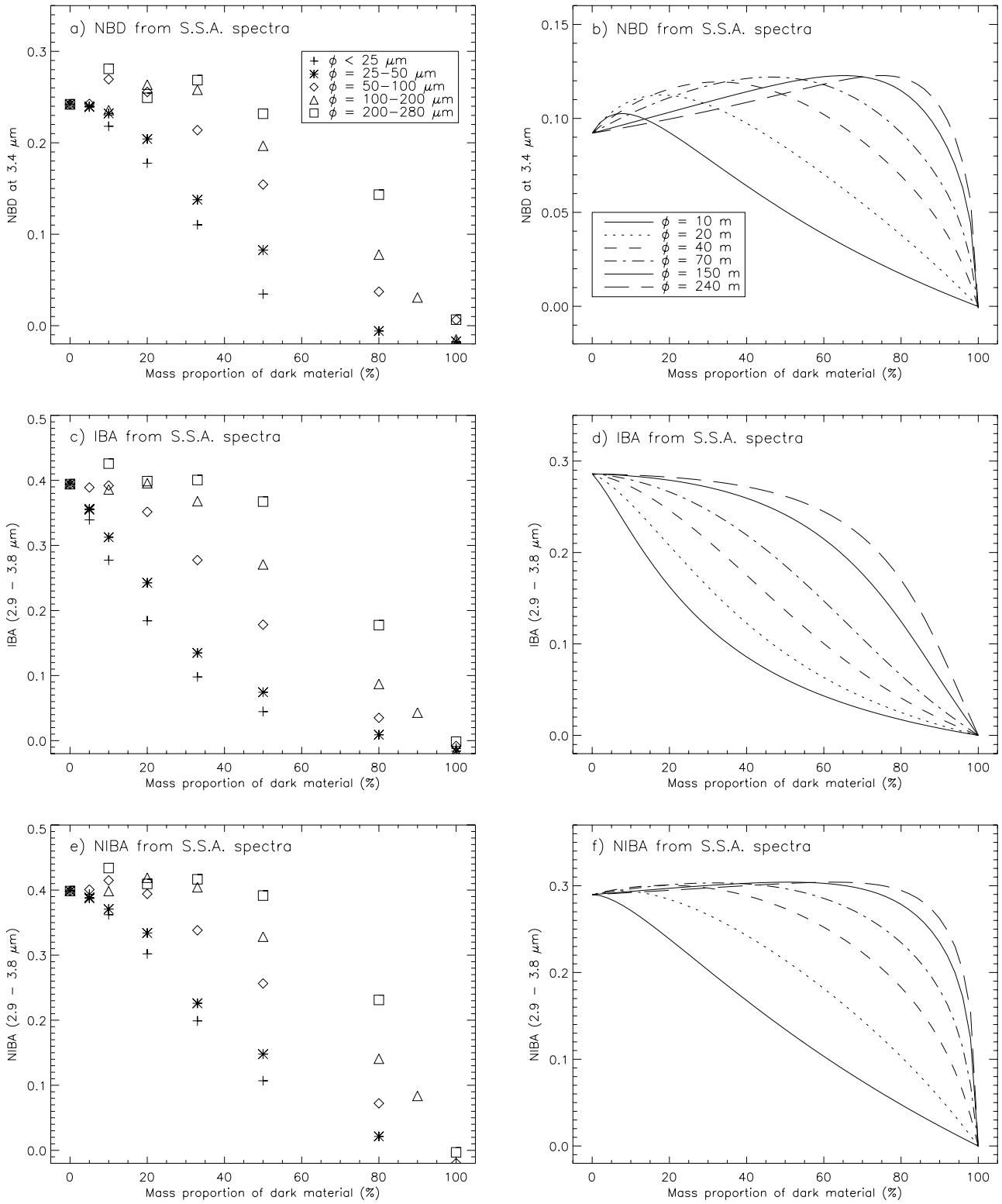

Figure 11. Same as Figure 10 but the band strength criteria are calculated from spectra converted to single-scattering albedo.

if some slight differences in the shape of the relationships between these criteria and the amount of anthracite can be noted. However, different materials are used for the laboratory measurements (STx-1/anthracite) and for the radiative transfer modeling (SWy-1/dark component). In addition, the unknown scattering phase functions of the materials are assumed to be isotropic in the model. Therefore, we correctly reproduce the general trends but did not expect to exactly fit the experimental data.

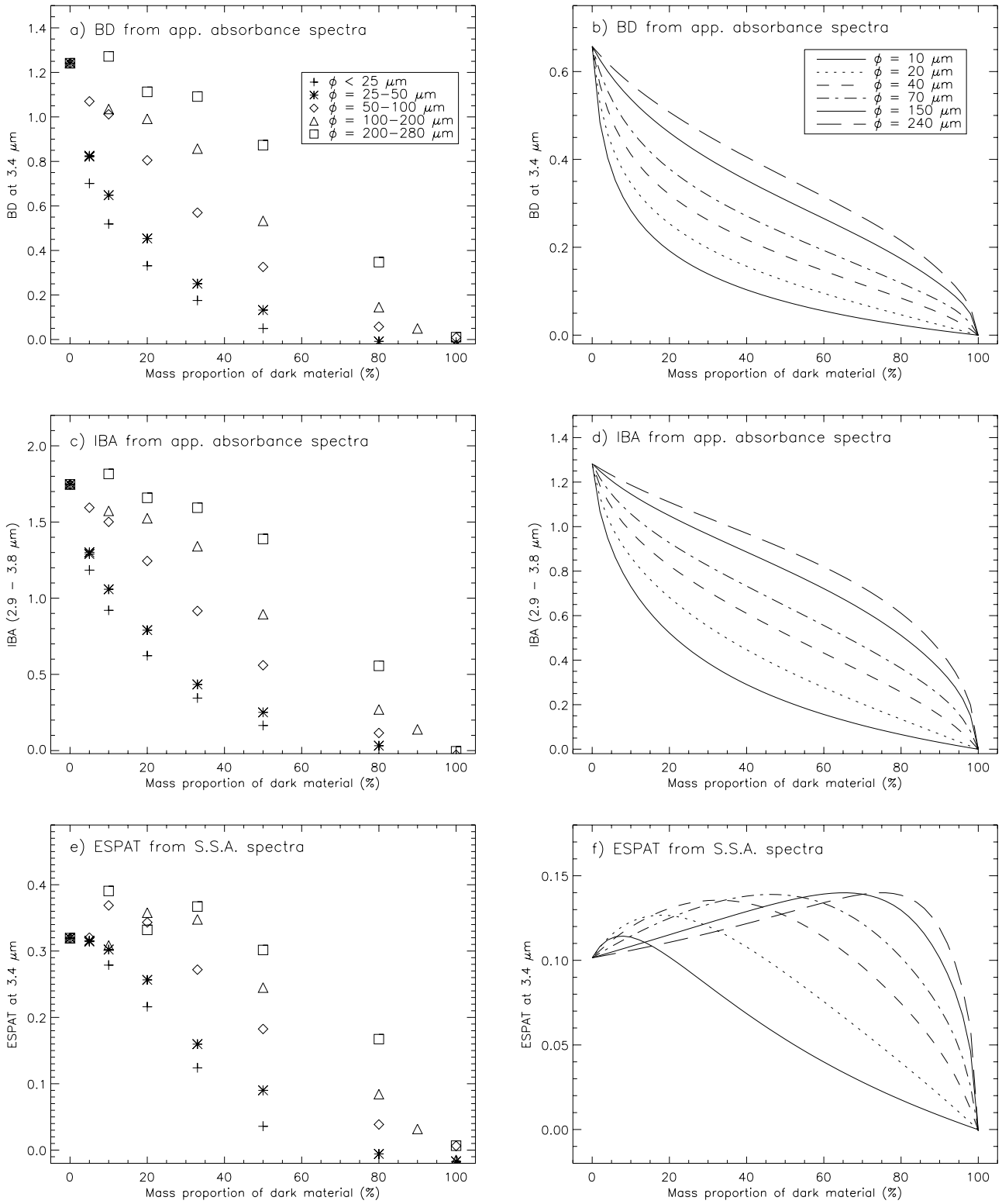

Figure 12. (a–d) Same as Figure 10 but the band strength criteria BD and IBA are calculated from spectra converted to apparent absorbance, whereas (e–f) the ESPAT criterion is calculated from spectra converted to single-scattering albedo.

[62] We tested the other spectral criteria in the hope of finding a better correlation between the 3-μm band strength and the sample water content. However, the strong particle size effects of the dark material are observed for all the tested band strength criteria, calculated from reflectance, apparent absorbance or single-scattering albedo spectra (Figures 10, 11, and 12). The ESPAT parameter (Figures 12e and 12f) and normalized band depth calculated from single-scattering

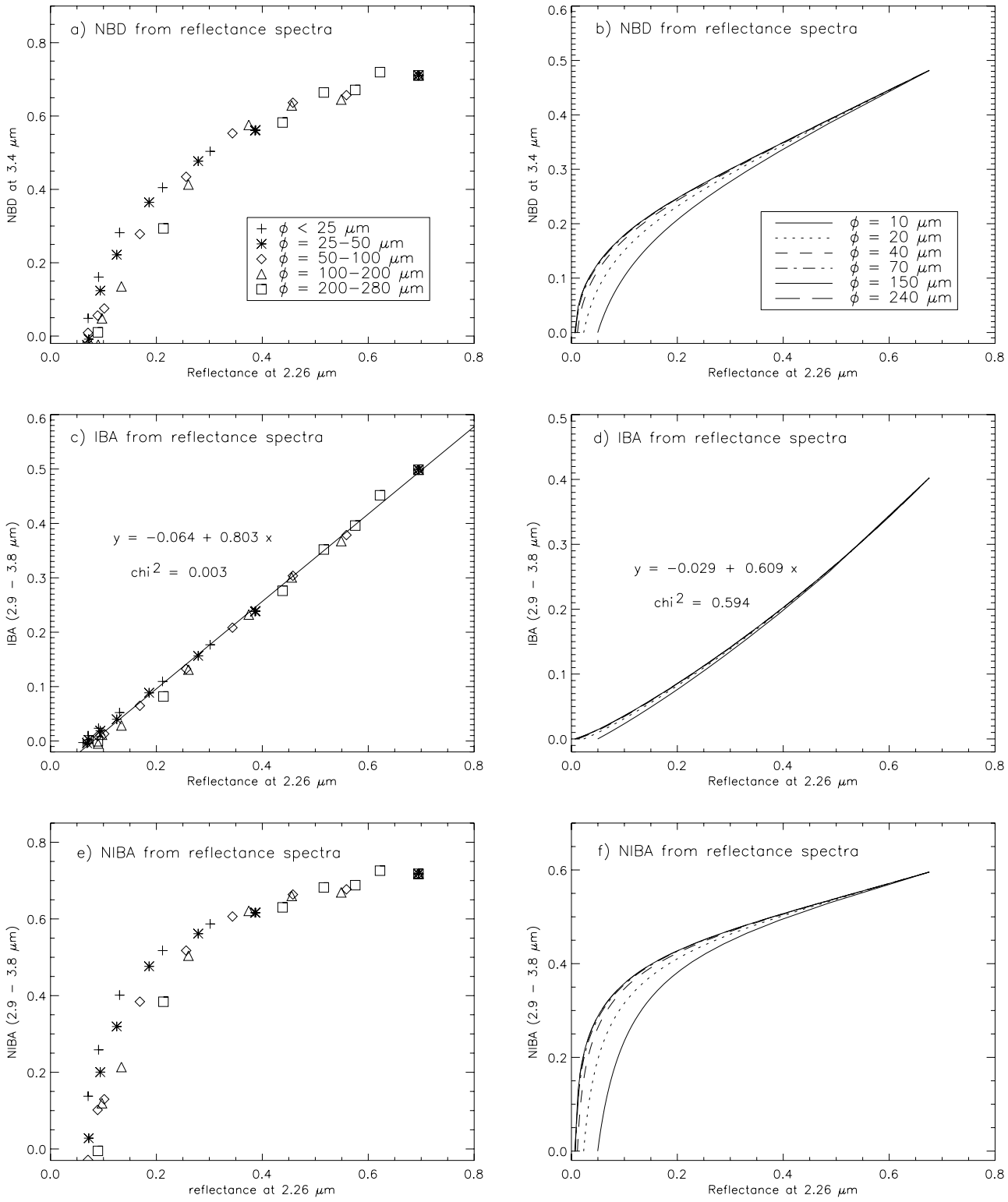

Figure 13. Granular mixtures. Evolution of the 3-μm band strength criteria (NBD, IBA, and NIBA) as a function of continuum reflectance level (at 2.26 μm) for different particle sizes of the dark component. All these criteria are calculated from reflectance spectra. (a, c, and e) Experimental results (mixture of STx-1 smectite and anthracite PSOC 1468). For IBA the best linear fit of the experimental data is superposed to highlight the strong linear correlation. (b, d, and f) Radiative transfer modeling (mixture of SWy-1 smectite and a synthetic dark material).

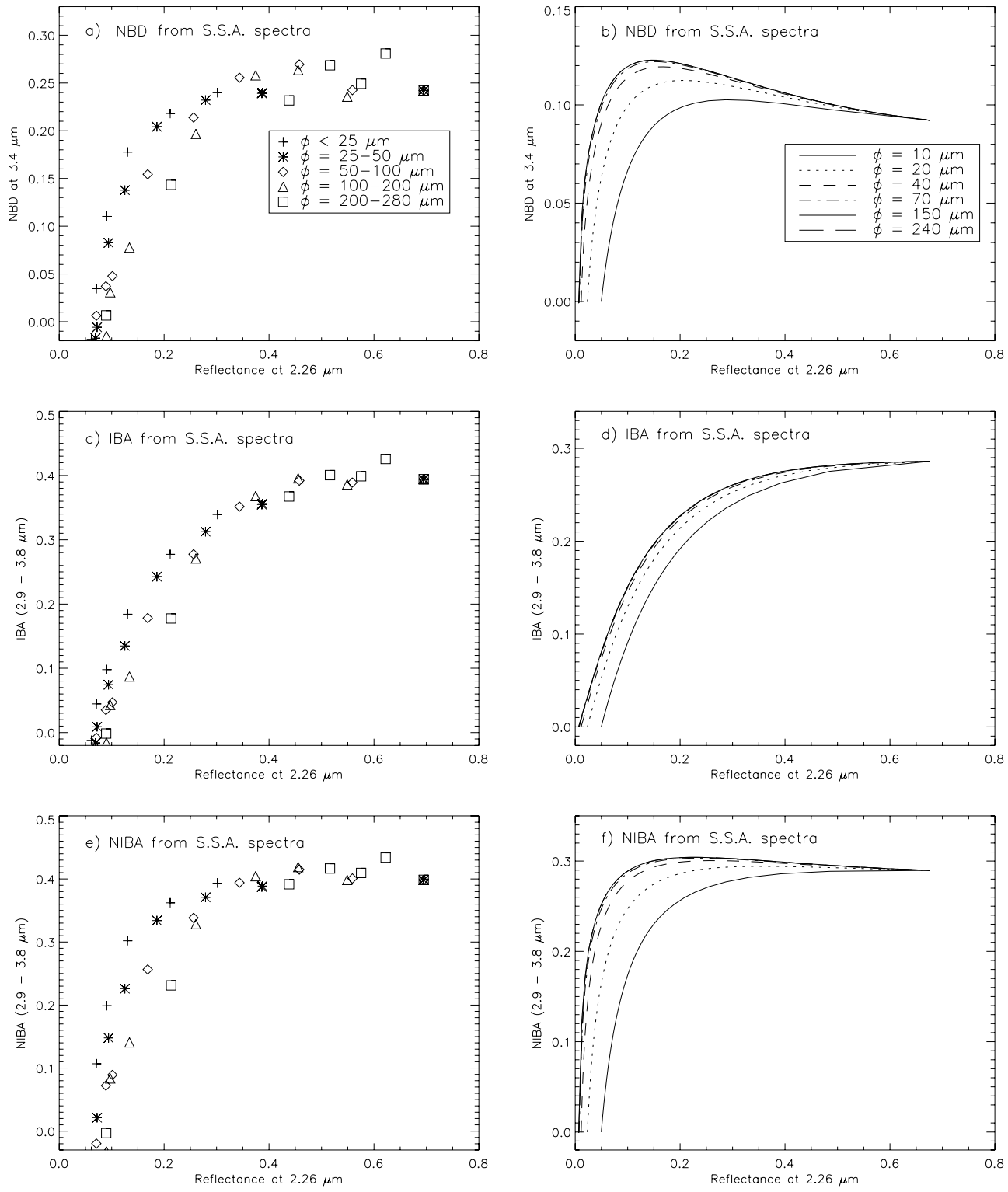

Figure 14. Same as Figure 13 but the band strength criteria are calculated from spectra converted to single-scattering albedo.

albedo spectra (Figures 11a and 11b) both show a more complex relationship with dark component/smectite mixing ratio. Another problem with these criteria is the relatively strong discrepancy that appears between measurements and modeling as soon as spectra are converted to single-scattering albedo, whereas they are consistent for criteria calculated from reflectance and apparent absorbance spectra. This problem has been already noted for the effects of particle size.

[63] As a global and positive correlation between the 3-μm band depth and the visible and near-infrared albedo has been found over Mars' surface [*Calvin*, 1997; *Murchie et*

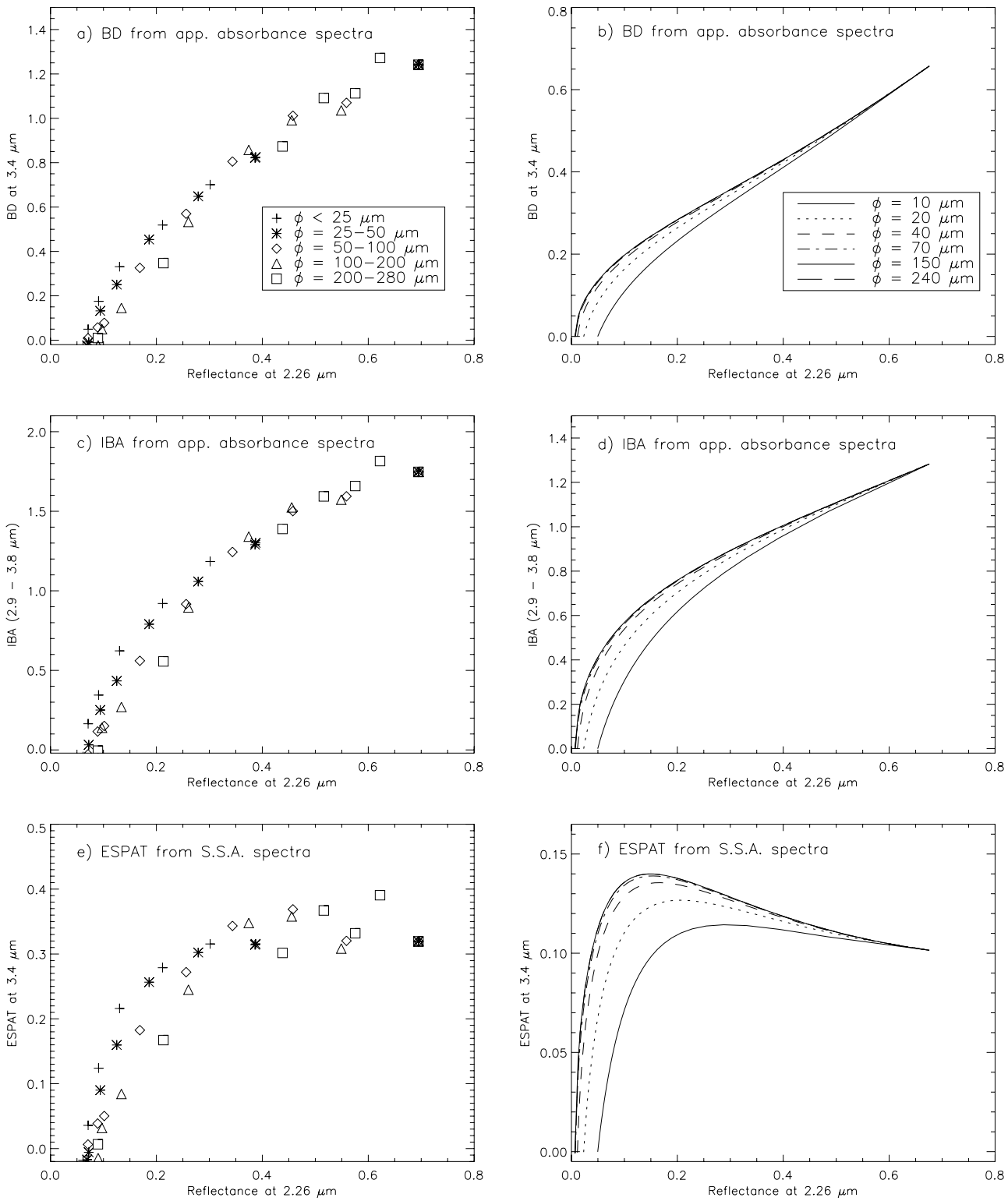

Figure 15. (a–d) Same as Figure 13 but the band strength criteria BD and IBA are calculated from spectra converted to apparent absorbance, whereas the (e–f) ESPAT criterion is calculated from spectra converted to single-scattering albedo.

al., 2000; *Jouglet et al.*, 2007] we investigate the origin of this behavior using our new experimental data set. Figures 13, 14, and 15 present the relationships between the various spectral criteria previously used to characterize the 3-μm band strength and the sample reflectance at one particular wavelength (2.26 μm) situated in the spectra continuum just before the wing of the 3-μm absorption band (Figure 5). We tested other continuum wavelengths, espe-

cially at the reflectance maximum between 1 and 2.2 μm, and always obtained the same type of relationships between band strength and continuum reflectance. For continuum reflectance larger than 0.1 we observe that all 3-μm band strength criteria have much smaller dispersions with particle sizes when plotted as a function of reflectance continuum level than versus sample water content (i.e., dark material content). However, dispersion is usually maximum when reflectance decreases below 0.05. This strong change in behavior is linked to the complex dependency of sample albedo with both the dark material particle size and proportion.

[64] The most striking point that emerges from these plots is the very strong linear correlation (see low χ^2 values in Figure 13c) between the IBA criterion estimated from measured reflectance spectra and the continuum reflectance, independently of particle size (Figure 13c). This should be compared with the extreme dispersion of this spectral criterion for different values of dark particle sizes but identical water content (i.e., same dark component amount) (Figures 10c and 10d). IBA derived from modeled spectra also presents a very linear relationship with continuum reflectance even if a slight curvature and a weak dependence for the smallest grain sizes ($\leq$10 μm) can be observed, especially for the lowest reflectance values (Figure 13d).

[65] From these mixing experiments, the infrared continuum albedo of the samples appears to be the only parameter that controls the 3-μm integrated band area. Despite this strong linear correlation, normalization by the continuum reflectance, leading to the NIBA criterion, is unable to remove the influence of albedo on the 3-μm hydration band (Figures 13e and 13f). This is linked to the fact that for the extreme ''mixture'' containing only pure anthracite the sample reflectance is small ($\sim$0.07) but not zero (Figures 9 and 13c). Thus, a simple normalization by the continuum reflectance produces a strong nonlinear effect, especially for low reflectance values (Figures 13e and 13f).

[66] When calculated from spectra converted to single-scattering albedo (Figures 14e, 14f, 15e, and 15f) or to apparent absorbance (Figures 15a and 15d), all the spectral criteria display a more or less pronounced nonlinear correlation as well as a larger dispersion with particle size than for IBA calculated from reflectance spectra. However, most of these criteria display an almost linear behavior with low dispersion for the higher-albedo samples. The range of validity of this linear correlation is particularly large for the band depth criterion calculated from absorbance spectra (Figures 15a and 15b). It should also be noted that the normalized band depth criterion calculated from single-scattering albedo spectra displays relatively constant values for high albedo. This supports the conclusions by *Milliken and Mustard* [2007a], who chose ESPAT as the best spectral criterion to retrieve the absolute water content of samples or surfaces independently of their albedo. However, the dispersion of the ESPAT values in our model (Figure 15f) becomes huge for low-albedo samples (<0.25), although our experiments tend to display stable but dispersed values (±15%) for albedo larger than 0.28 (Figure 15e). Dispersion between the different curves is mainly attributed to the different amounts of dark material and the effects of particle size that are particularly strong for spectra criteria using single-scattering albedo (see section 3.1.2 and *Milliken and Mustard* [2007b]). Effects of particle size become more pronounced as more and more dark material is added in the mixture. As already noted before, conversion to single-scattering albedo seems to overemphasize small discrepancies between experiments and modeling, and thus probably induces unreliable determinations of the water content.

[67] The strong linear correlation found between IBA and the continuum reflectance (Figure 13c) points out IBA as the most promising spectral criterion to separate the effects of water content and albedo on the 3-μm band strength when this band is saturated in the 2.9-μm region. However, to be useful, this correlation should be reproducible with other hydrated materials and different levels of hydration. To investigate the effect of water content, we prepared granular mixtures of different amounts of anthracite with gypsum (particles <25 μm) and altered volcanic tuff (particle size fraction: 50–100 μm). For these two sets of experiments, anthracite was not separated in different particle size fractions. Reflectance spectra of these two series of mixtures are presented in Figure 16.

[68] The IBA criterion again displays a strongly linear correlation with reflectance at 2.26 μm for both the gypsum-anthracite and volcanic tuff-anthracite mixtures, as shown by the low values of the χ^2 parameter (Figure 17). The slope and origin ordinate are different for each of the three hydrated minerals, reflecting different values of IBA for the three pure hydrated minerals. These differences in IBA values are related to variations of water content between minerals but also to variations of particle size (see section 3.1) and of chemical and mineralogical compositions [*Milliken and Mustard*, 2005]. Therefore, while the linear correlation (and its deviations) between IBA and continuum reflectance will be probably invaluable to discriminate the origin of band strength variations (effect of albedo versus real mineralogical or water content variations), it should not be considered as a good tool to derive maps of absolute values of surface water content if the mineralogical composition and/or particle size presents large spatial variations.

[69] For the smectite/anthracite mixture, normalization of IBA by the continuum reflectance generates a nonlinear relationship between NIBA and continuum reflectance (Figure 17b). However, in the case of the volcanic tuff, the nonlinearity of this relationship is less marked than for smectite and gypsum. Difference between these samples is linked to the strong difference in absolute water content of the pure hydrated material (see Table 1) that leads to a smaller contrast of hydration between volcanic tuff (2.3%) and anthracite (<1%) than between smectite (14.6%) or gypsum (20.7%) and anthracite. In a similar way, contrast of albedo between volcanic tuff and anthracite is also reduced compared to contrast of albedo between gypsum or smectite and anthracite.

3.2.2.2. 1.9-μm Hydration Band

[70] Normalized band depth calculated at 1.9 μm from reflectance spectra presents the same kind of evolution than the 3-μm band strength as a function of mixing ratio and dark component particle size (Figure 18). The large dispersion between band strength values calculated for a single mixing ratio but different dark component particle size fractions is potentially a major source of error in water

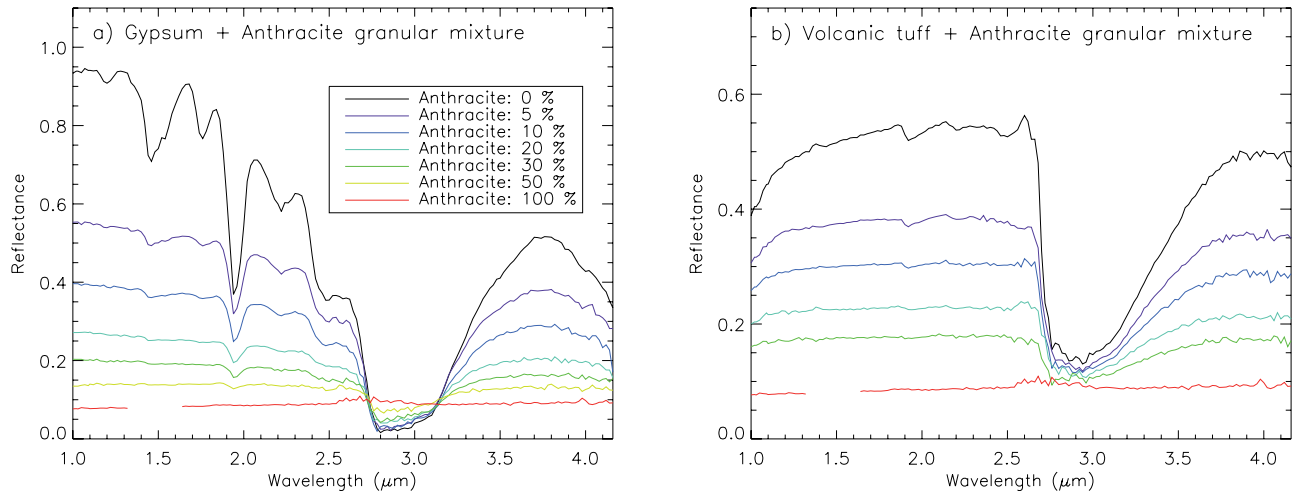

Figure 16. Reflectance spectra of mixtures between (a) gypsum and anthracite and (b) volcanic tuff (50–100 μm particle size fraction) and anthracite.

content determinations. For example, in the case of the 1.9-μm band calculated from measured reflectance spectra for a mixing ratio of 50%, value of NBD decreases by a factor of 10 between mixtures with the highest and lowest anthracite particle size. Relative variations are smaller on modeling results but general trends are identical between experiments and modeling. BD in apparent absorbance at 1.9 μm gives exactly the same results as NBD calculated from reflectance spectra. Normalized band depth calculated from single-scattering albedo reveals a very complex relationship with mixing ratio and dark component particle size. These complex relationships yield to a very strong dispersion among materials with identical water content but different continuum reflectance level.

[71] We also plotted the 1.9-μm band strength values as a function of continuum reflectance level as we did for the 3-μm band. Results are shown on Figure 19 for measurements and modeling. On experimental results, NBD at 1.9 μm calculated from reflectance spectra (Figures 19a and 19b) presents a roughly linear trend with continuum reflectance level. Results from modeling show a relatively similar general trend, but a larger dispersion can be noted between mixtures synthesized with different dark component particle sizes. This discrepancy between experiments and modeling is probably partly due to the difference of water content (and then absolute value of band strength) between the STx-1 and SWy-1 smectites (measured and modeled, respectively). However, a part of the discrepancies is also likely to be due to the incapacity of the model to exactly reproduce the complexity of light scattering in natural mixtures implying such large variations of albedo and particle size. A high dispersion is evident for small band strengths (SWy-1 smectite) but it rapidly decreases and disappears as band strength increases (1.9-μm band for the STx-1 smectite and 3-μm band for all samples).

[72] BD in apparent absorbance at 1.9 μm (Figures 19e and 19f) gives the same results as NBD at 1.9 μm from reflectance spectra whereas normalized band depth calculated from single-scattering albedo spectra (Figures 19c and 19d) shows an extremely complex relationship with continuum reflectance and, as always, a strong discrepancy between results from experiments and modeling.

3.2.3. Geographic Mixtures and Intrinsic Variations of Particle Optical Properties

[73] In all the experiments and modeling presented so far, the variations of sample albedo were always obtained by granular mixtures of high- and low-albedo materials. However, on planetary surfaces, other physical processes are also responsible for albedo variations. Therefore, it is necessary to study the effect of albedo on band strength using different methods to see if conclusions obtained with granular mixtures remain valid. Using numerical modeling, we study the effects of geographic mixtures and variations of intrinsic optical properties of mineral grains on the H_2O band strength.

[74] Spatial mixtures may occur at the pixel level: the different materials are not intimately mixed at the grain level but cover areas that cannot be spatially resolved by the instrument. The reflectance spectra of such surfaces correspond to linear combinations of the different end-members reflectance spectra weighted by their spatial coverage.

[75] Variations of the intrinsic optical properties of individual mineral grains are also a major source of surface albedo variations. Reflection and absorption of the particles can be modified by a change in chemical composition (e.g., presence of a strongly absorbing element inside a mineral structure). One can simulate at first order such variations of minerals optical properties by linearly mixing the optical constants of a pure mineral with synthetic optical constants of a spectrally neutral featureless absorber [*Quirico et al.*, 1999]. The fundamental flaw of the linear optical constants linear combination is that changes in band position caused by substitution of chemical elements in the mineral structures are not modeled. However, this is not a problem in the case of our study as we are only interested in the effect of albedo.

[76] We used the radiative transfer model to calculate reflectance spectra corresponding to geographic mixtures and intimate mixtures in the following way:

[77] 1. Reflectance spectra of pure smectite and pure dark component are independently calculated from the optical

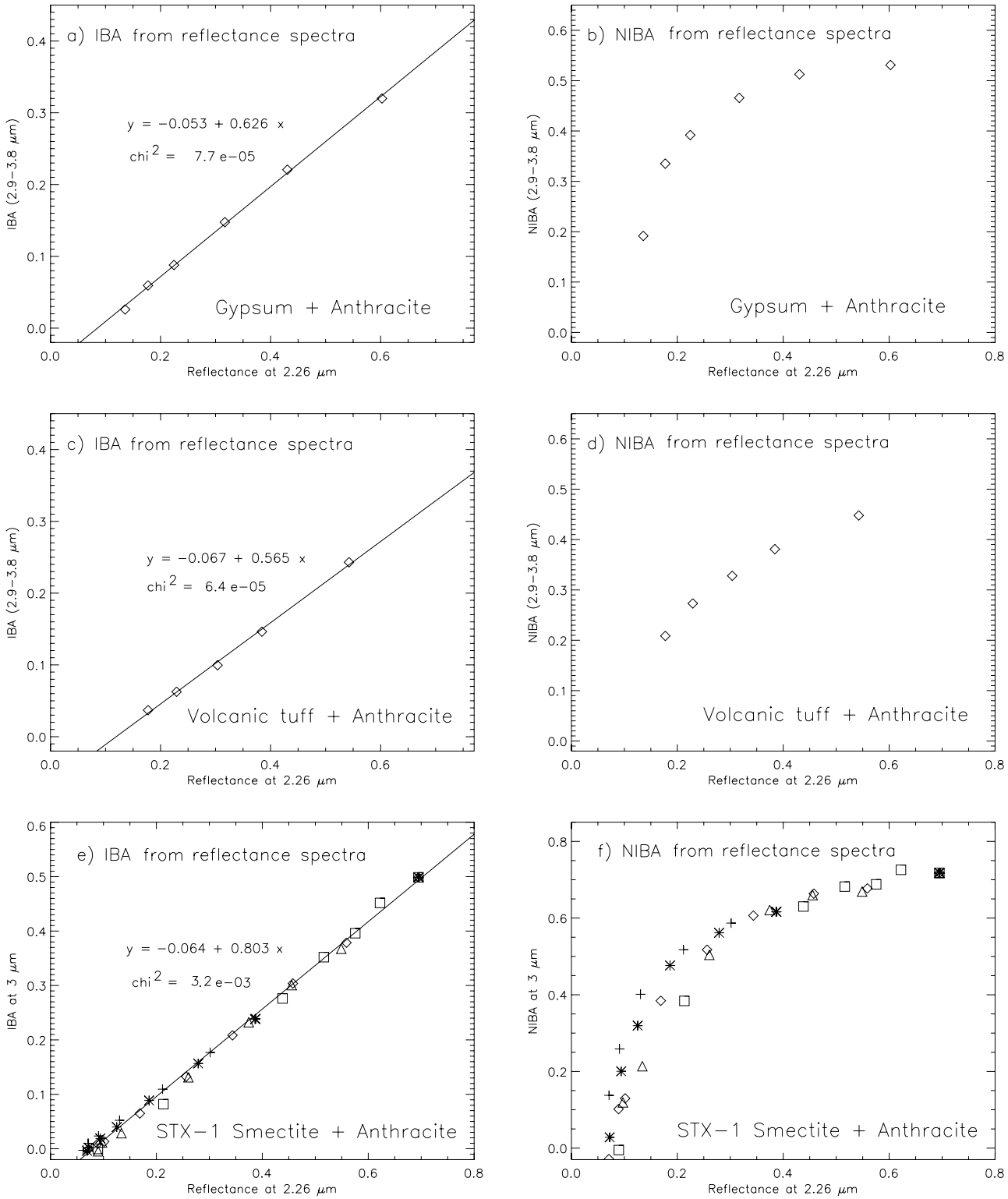

Figure 17. Evolution of the 3-μm band strength criteria (IBA and NIBA) as a function of continuum reflectance level (at 2.26 μm). Experimental results for granular mixtures of (a–b) gypsum (particle size <25 μm) and anthracite and (c–d) volcanic tuff (50–100 μm particle size fraction) and anthracite. (e–f) Results for the same criteria calculated for granular mixtures of smectite and anthracite and presented on Figure 12 are also plotted to permit a direct comparison between the different materials. When IBA is plotted versus reflectance in the continuum (Figures 17a, 17c, and 17e), we superpose to the data the best fit line. Equations and chi^2 values are provided for each best fit line.

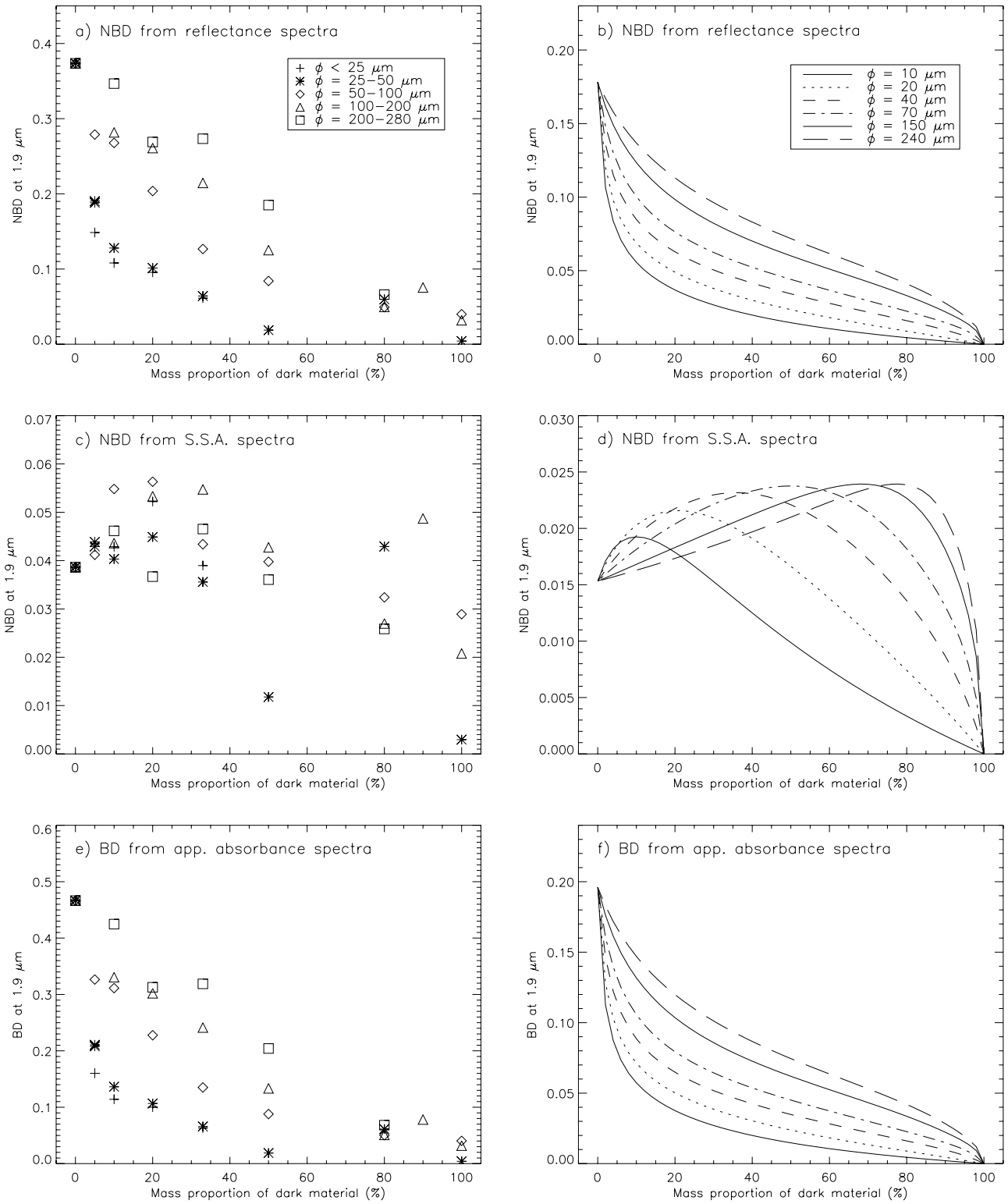

Figure 18. Granular mixtures. Evolution of the 1.9-μm absorption band strength criterion (NBD) as a function of dark material/smectite mixing ratio for different particle sizes of the dark component. NBD is calculated from reflectance, single-scattering albedo and apparent absorbance spectra. (a, c, and e) Experimental results (mixture of STx-1 smectite and anthracite PSOC 1468). (b, d, and f) Radiative transfer modeling (mixture of SWy-1 smectite and a synthetic dark material).

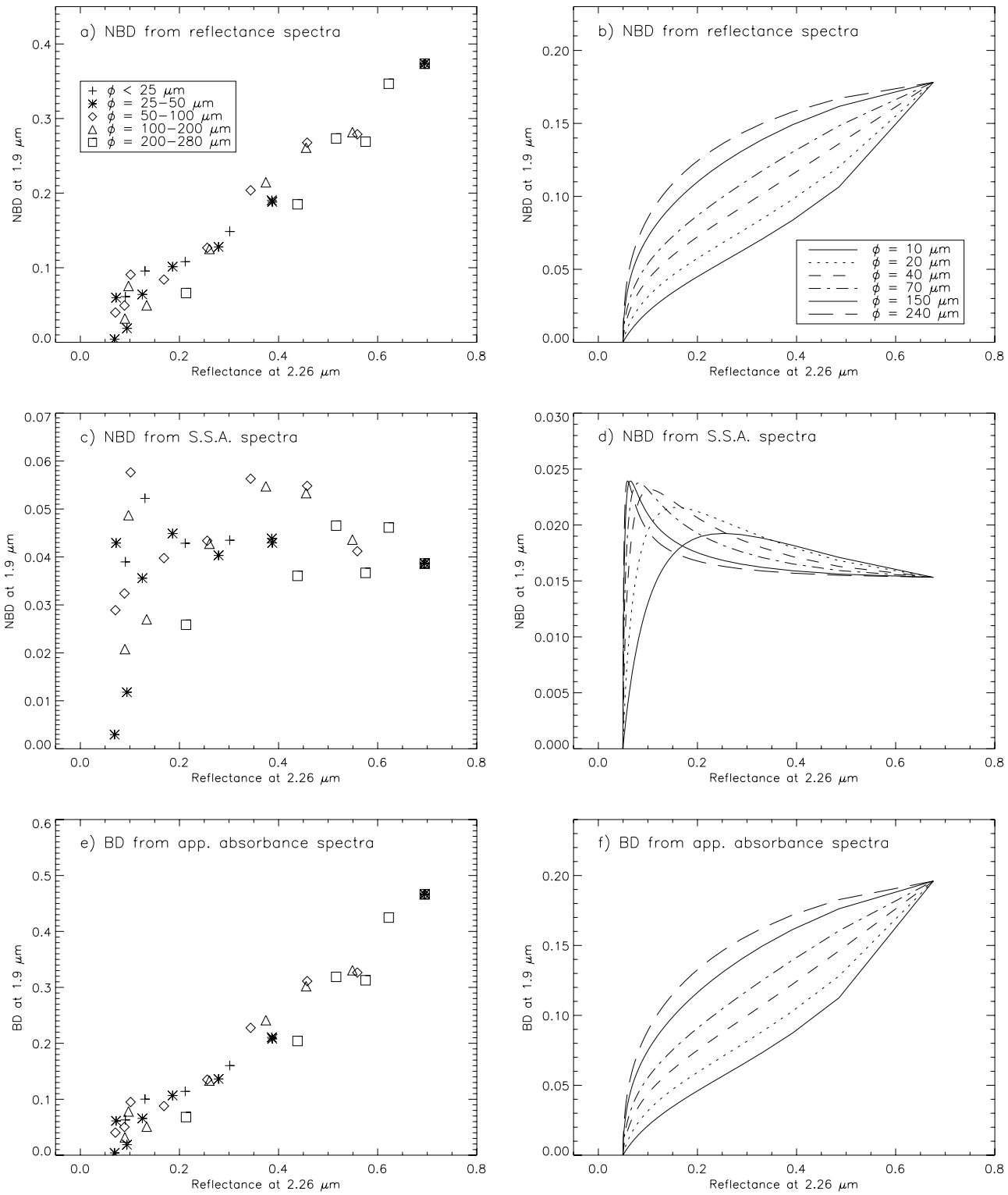

Figure 19. Same as Figure 18 but for the evolution of the 1.9-μm absorption band strength criteria as a function of the continuum reflectance level (at 2.26 μm).

constants using a constant particle size of 20 μm. Then, the reflectance spectra of the two end-members are linearly combined in various proportions.

[78] 2. Synthetic optical constants are calculated by linear combinations of the two end-members optical constants in various proportions. Then, reflectance spectra are calculated from the new synthetic optical constants using the radiative transfer model with a constant particle size of 20 μm.

[79] Figure 20 shows a comparison of the evolutions of different 3-μm band spectral criteria as a function of dark material proportion or continuum reflectance for the three kinds of mixing used to vary sample albedo: spatial mixture,

granular mixture, and combination of optical constants. It is evident from all the plots that spatial mixtures and variations of particles intrinsic optical properties behave like the two extreme cases of the granular mixtures (Figures 20a and 20d). The behavior of band strength for spatial mixtures is similar to the behavior of a granular mixture with very large dark component particles whereas it is similar to a granular mixture with very small dark component particles in the case of particle intrinsic optical properties variations.

[80] A linear relationship between IBA and the continuum reflectance is also observed for these two mixing processes with slopes and origin ordinates close to what is observed in the case of granular mixtures (only a slight curvature occurs for optical constant mixing) (Figures 20e and 20f). Low values of χ^2 indicate a correct correlation in both cases even if a slightly larger value of χ^2 for optical constants mixing than for other plots indicates a minor discrepancy with the usual linear trend. Therefore, this interesting property appears to be valid for any process that produces variations of the infrared albedo of samples.

[81] The 1.9-μm band displays a very different behavior as can be seen on Figure 21. Normalized band depth presents an almost linear correlation with continuum reflectance in the case of variations of particles intrinsic optical properties (Figure 21b) whereas band depth displays a linear relationship with continuum reflectance in the case of spatial mixtures (Figure 21d). In both cases, very low values of χ^2 indicate excellent correlations. Therefore, in the case of the weak 1.9-μm band, no general trend that could provide a systematic way to handle the correlation of this band with surface infrared albedo can be extracted from our physical or numerical experiments. On the other hand, these clearly different behaviors could be used to get insight into the mode of mixing that control the spatial variations of surface albedo.

4. Discussion

[82] Results from experiments and modeling demonstrate the strong effects of albedo and particle size on the H_2O near-infrared absorption bands. Good consistency between experiments and models demonstrates that the observed band strength variations are well explained by the physics of radiative transfer in particulate surfaces and could potentially be predicted if all the needed parameters were simultaneously known. However, this is never the case when dealing with planetary surfaces remote sensing. All the processes described in this study that affect the strength of hydration bands of a material at constant water content complicate the interpretation of planetary surfaces near-infrared reflectance spectra and the extraction of information related to water of hydration.

[83] Strong effect of particle size on the 1.9- and 3-μm hydration band strengths are shown with good consistency between experiments and modeling (for smectites) over the range of particle size (above 10 μm) where geometrical optics laws are valid. In the case of the 1.9-μm band, experimental data by *Cooper and Mustard* [1999] show that the band strength continues to decrease for finer particles. Therefore, NBD at 1.9 μm calculated on reflectance spectra may vary by a factor of 10 between micrometer-sized and millimeter-sized grains at a constant hydration state. This puts important constraints on the detection limits of this band from planetary surfaces. The broad 3-μm band presents smaller variations as a function of particle size. However, to our knowledge, no experimental data exist for particle sizes of a few micrometers or less. An experimental study conducted in this range of particle sizes would probably reveal a further decrease of the 3-μm band strength as observed for the 1.9-μm and other weak bands [*Cooper and Mustard*, 1999]. Conversion of reflectance spectra to apparent absorbance or single-scattering albedo do not reduce effects of particle size variations but, on the contrary, often increase those effects. *Yen et al.* [1998] found that conversion from reflectance to apparent absorbance reduced the effect of particle size on band strength for particles between less than 38 and 150 μm. Our own results do not confirm this point and, on the contrary, show a larger influence of particle size on criteria derived from apparent absorbance than on criteria derived from reflectance spectra. A possible explanation for this difference is that *Yen et al.* [1998] use very dark materials to test the effect of particle size (Basalt + Palagonite mixture with reflectance between 0.07 and 0.16 in the continuum) whereas all samples measured in our study were relatively bright. As conversion from reflectance to apparent absorbance is logarithmic; it has a very strong effect on low reflectance values but only small effects on larger reflectance values. Therefore, effects of this conversion on band strength will be very different if reflectance both in the band and in the continuum are low or if reflectance is low in the band but high in the continuum.

[84] In a similar way, the strong correlation of all the calculated spectral criteria with sample albedo induces severe bias in the mapping of the water of hydration band strength on planetary surfaces. An implication of these results can be formulated in terms of detection limit for mineral hydration. Mineralogical maps extracted from reflectance spectra are produced by mapping areas where the strength of a particular hydration band is larger than the detection limit of this band (usually related to instrumental noise). These maps are then generally interpreted in a binary way as presence or absence of mineral hydration and discussed in terms of geological processes responsible for the spatial distribution of hydration. However, the effects of particle size and albedo on the band strength are rarely taken into account. The detection limit of weak hydration bands should be considered as highly dependant on both these parameters. High-albedo surfaces with large particles allow the detection of tiny amounts of water whereas dark areas composed of fine particles could retain large quantities of water without displaying strong enough hydration bands to be detected.

[85] Spatial variations of surface albedo and particle size on a planetary surface introduce severe bias in the water detection and in the mapping and interpretation of its abundance distribution. Therefore, a map of hydration band strength cannot be directly interpreted in terms of water of hydration as long as the effects of these two parameters are not corrected.

[86] To complicate the situation, it must be noted that the effects of particle size and surface albedo are not independent on planetary surfaces whereas they can easily be studied separately in laboratory experiments and radiative

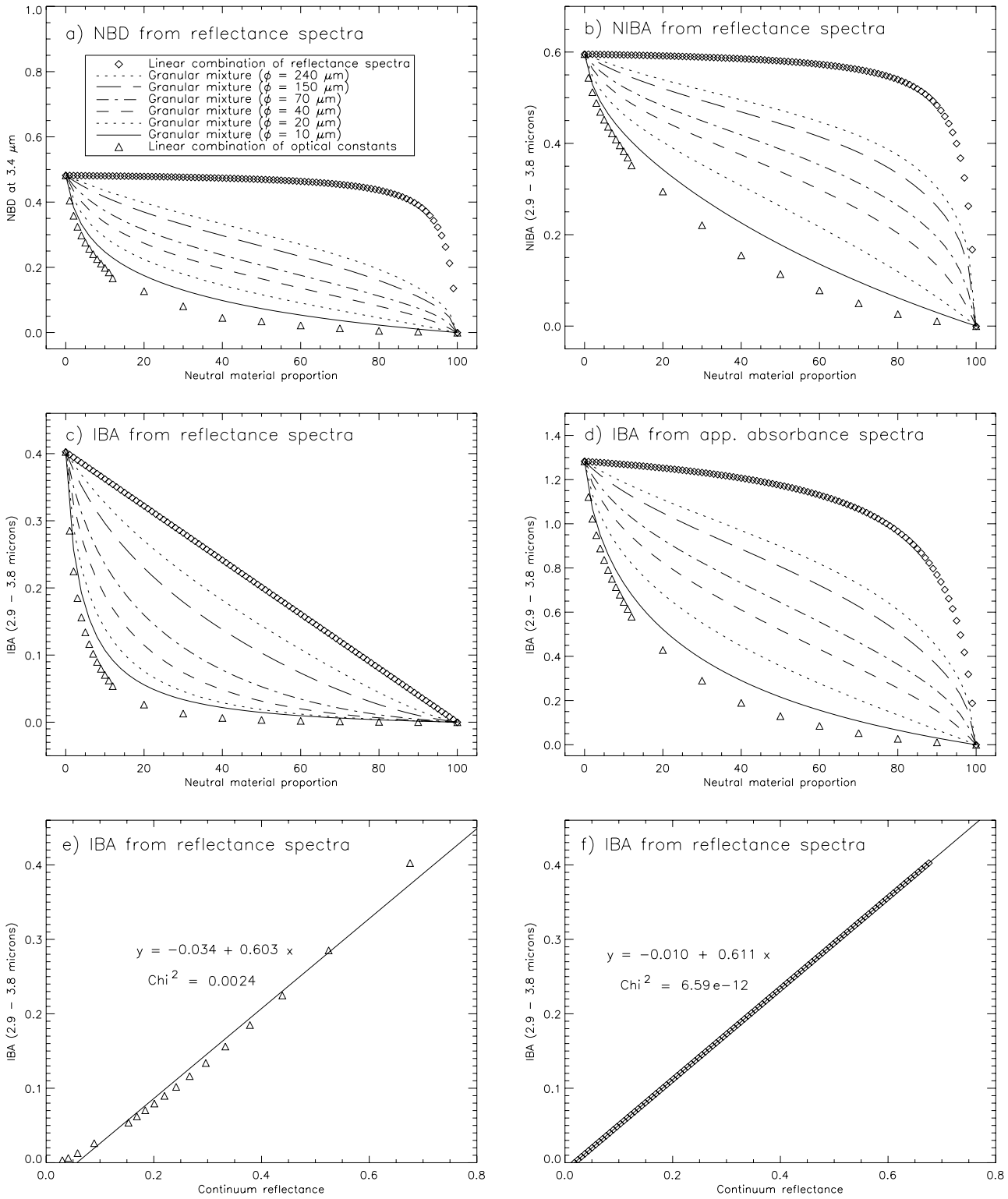

Figure 20. Evolution of 3-μm band strength criteria as a function of (a–d) dark material proportion and (e–f) continuum reflectance at 2.26 μm. Results from radiative transfer modeling of granular mixtures (dark particle size fractions, mass proportion); intimate mixture (linear combination of the optical constants of the two components, volume proportion); and spatial mixture (linear combination of the reflectance spectra of the two components, surface proportion). The straight line in Figures 20e and 20f are the best linear fits of the data.

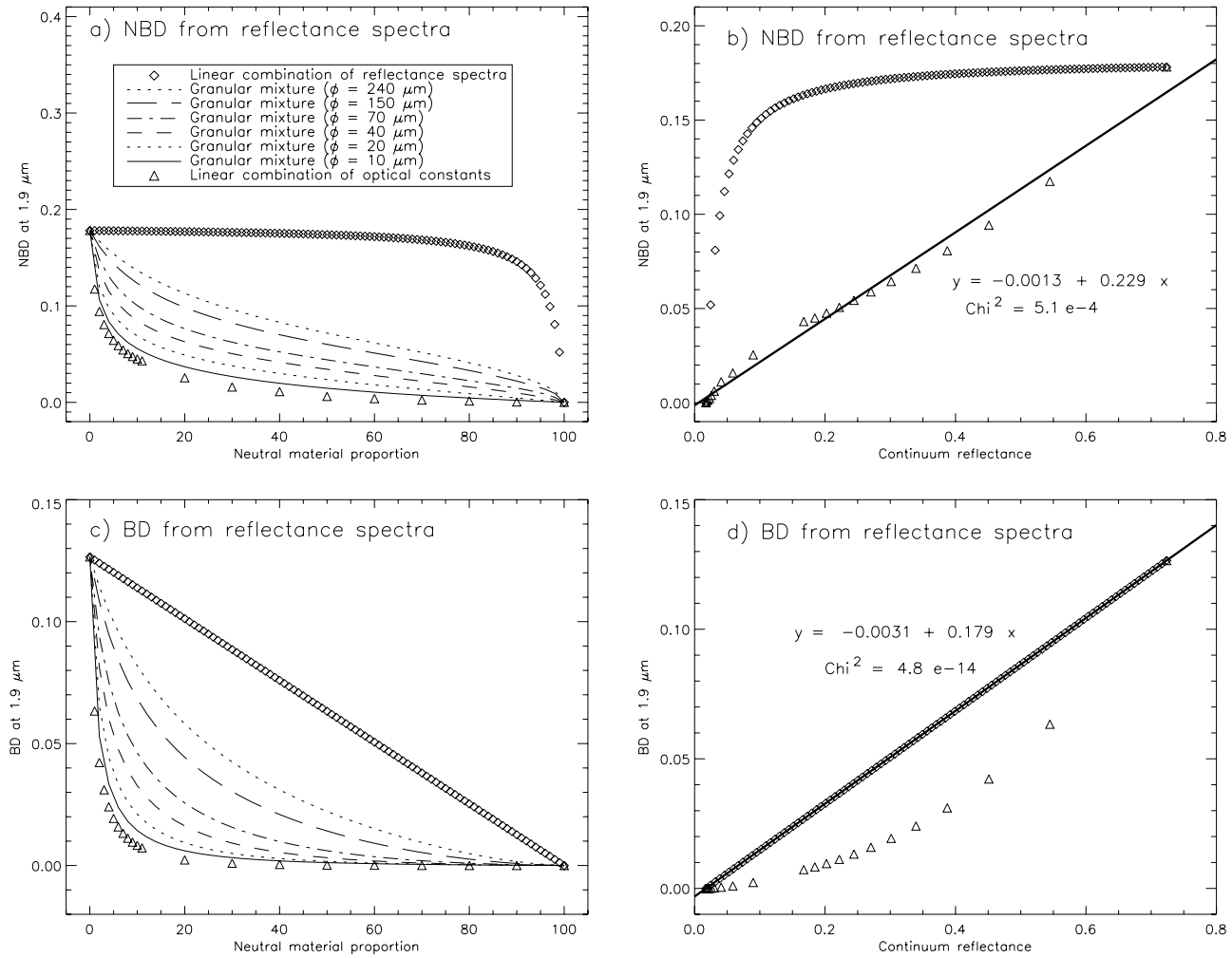

Figure 21. Same as Figure 20 but for the evolution of 1.9-μm band strength NBD and BD criteria as a function of (a and c) dark material proportion and (b and d) continuum reflectance at 2.26 μm. The straight line in Figures 21b and 21d are the best linear fits of the data.

transfer modeling. For example, band strength is positively correlated to surface albedo but variations of particle size introduce a negative correlation between band strength and surface albedo (band strength decreases and continuum reflectance increases when particle size decreases). On a real planetary surface, these two opposite correlations are superposed, leading to an even more complex relationship between surface albedo and band strength.

4.1. How to Handle the Band Strength/Albedo Correlation

[87] Correlation between band strength and albedo is prominent in laboratory experiments, radiative transfer modeling, and on planetary surfaces. This effect has been noted by many authors in the case of Mars (see section 1).

[88] On the basis of laboratory experiments, *Milliken and Mustard* [2007a] proposed the use of the ESPAT criterion at 2.9 μm to estimate material absolute water content because they found it to be independent of the infrared continuum reflectance level. However, they also show that this criterion is very sensitive to particle size [*Milliken and Mustard*, 2007b]. As this criterion can only be used when absorption band is not saturated at 2.9 μm, very few of our own measurements can be used to try to test this conclusion. However, the volcanic tuff spectra (pure and mixed with anthracite) are not saturated in the 2.9 μm region (Figures 6 and 16). Therefore, we calculated the ESPAT criterion at 2.9 μm after conversion of these spectra to single-scattering albedo as described by *Milliken and Mustard* [2007a]. Figures 22a and 22b present the ESPAT criterion plotted versus tuff/anthracite mixing ratio and versus volcanic tuff mean particle size, respectively. These results are in very good agreement with the results of *Milliken and Mustard* [2007a, 2007b] as we observe a clear linear relationship ($\chi^2 < 10^{-4}$) between ESPAT at 2.9 μm and tuff/anthracite mixing ratio (proportional to the sample water content) and a strong decrease of ESPAT when particle size of the sample decreases. In materials for which the H_2O band is saturated at 2.9 μm, we tried to calculate the same spectral criterion at 3.4 μm, in the right wing of the absorption band. However, in that case, ESPAT shows a significant correlation with continuum reflectance, at least for albedo below 0.4 (Figure 15e). Above this value our experiments display a significant dispersion (±15%) in the ESPAT values. As discussed by *Milliken and Mustard* [2007a], the highly

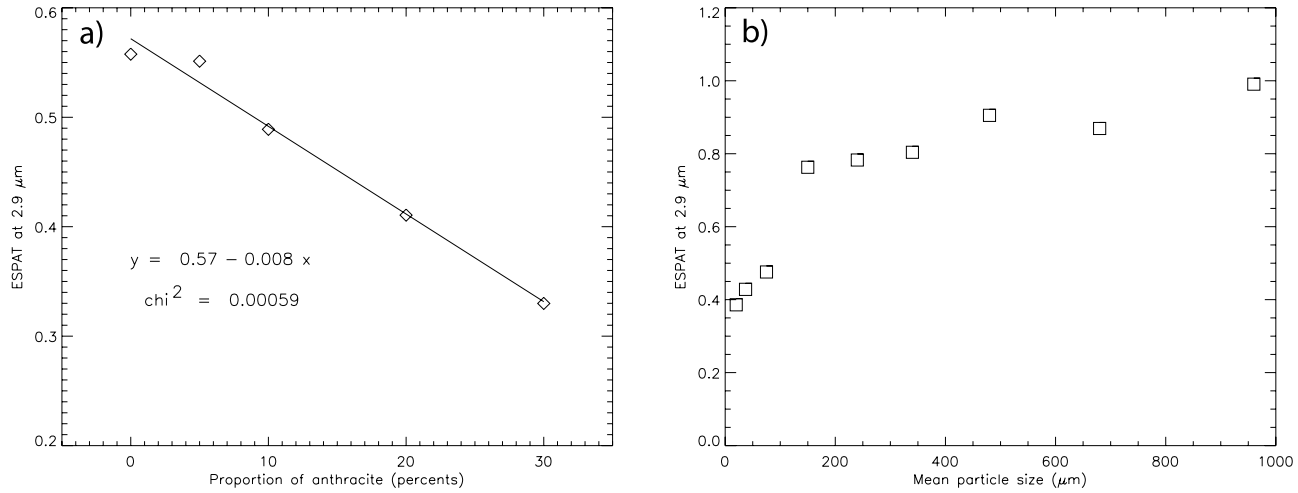

Figure 22. ESPAT spectral criterion calculated at 2.9 μm from single-scattering albedo spectra of the volcanic tuff. (a) Values of the ESPAT criterion plotted versus mixing ratio between volcanic tuff and anthracite. (b) Values of the ESPAT criterion plotted versus particle size of the pure material.

nonlinear conversion from very low reflectance values to single-scattering albedo can lead to large uncertainties. A comparison between our experiments and models also point to a similar inversion problem for high-albedo materials (Figures 15e and 15f).

[89] Using the experimental and modeling results presented in section 3, we propose another method to treat the dependence of the 3-μm band strength on sample albedo. It is based on the strong and highly linear correlation of the IBA calculated from reflectance spectra with the reflectance in the infrared continuum (Figures 13c and 13d). A simple normalization by the continuum reflectance level (NIBA) being inefficient to remove the dependency (Figures 13e and 13f), we propose to only consider the deviations from the linear trend as indicative of water content variations. However, this method requires a hyperspectral data set containing a large number of pixels with enough albedo variability to isolate the linear trend as the first-order variability inside the data set. The various data sets acquired on the Martian surface are particularly good candidates to test our method. *Calvin* [1997] has shown that the criterion she called integrated band depth (similar to our integrated band area criterion) presents a strong linear correlation with continuum reflectance on the Mariner 6/IRS data set. In a preliminary analysis of the OMEGA/Mars express observations, *Pommerol et al.* [2007] found a very strong linear correlation between the IBA criterion and the reflectance at 2.26 μm with a slope and an origin ordinate similar to the one determined in the experiments presented in this paper. Normalization by the value of reflectance in the continuum shortwave the 3-μm band (NIBA) results in a "logarithmic-like" relationship that looks similar in OMEGA data and experimental and modeling results (Figures 13e and 13f). *Jouglet et al.* [2007] obtain this same type of first-order relation between NIBA and continuum reflectance for a large number of OMEGA observations. *Calvin* [2007] also observes a strong correlation between apparent absorbance at 2.9 μm and reflectance at 2.3 μm for four ISM hyperspectral data cubes. She proposes to consider the difference between the data points and a second-order polynomial fit as a proxy of surface material water content deviation. This method shows a good agreement of the locations of high hydration with structurally hydrated minerals identified by the TES and OMEGA instruments.

[90] The method that we propose here is very similar to the one described by *Calvin* [2007] but uses the IBA criterion instead of apparent absorbance because it correlates linearly with surface albedo (Figures 13c and 13d) and avoids fitting a polynomial function to the data set. In addition, IBA is much less dispersed at fixed albedo relative to dark component grain size variations than apparent absorbance (Figures 14a and 14b). Therefore, we expect smaller uncertainties. On the other hand, the use of IBA is restricted to data sets with spectra covering the whole spectral range of the 3-μm absorption whereas the method using apparent absorbance only requires measurement at one wavelength in the absorption band and one in the infrared continuum.

[91] However, it must be noted that the method proposed here can only be applied statistically on a large number of pixels to extract the general trends between continuum reflectance and IBA. Then, contrary to the method used by *Milliken et al.* [2007], the method that we propose here cannot capture all variations in surface hydration at the instrument spatial resolution.

[92] Derivation of absolute water content from the 3-μm H_2O band using ESPAT at 2.9 μm is only possible if the absorption band is not saturated in this area. Even in the case of strong but not saturated absorptions, the highly nonlinear conversion from reflectance to single-scattering albedo and derivation of the spectral criterion at the maximum of the absorption could lead to large amplifications of uncertainties. On the contrary, the linear correlation between IBA and continuum reflectance is only valid for strong absorptions, saturated or close to saturation at the maximum of the absorption. Thus, it is probably more appropriate for materials with higher water content. However, it must also be kept in mind that IBA is dependent on sample nature and chemistry [*Milliken and Mustard*, 2005]. Therefore, the method that we propose to discriminate effects of albedo

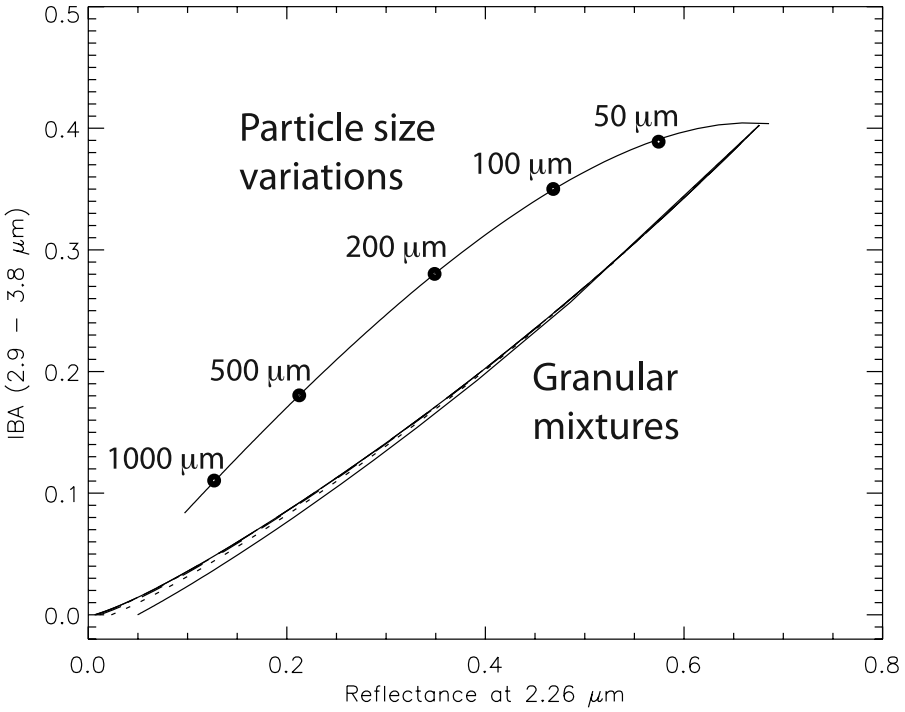

Figure 23. Relationship between the 3-μm IBA and the continuum reflectance level (at 2.26 μm) of the sample. Comparison between the effect of particle size variations and that of granular mixtures (bright plus dark materials). Data obtained from radiative transfer numerical modeling using optical constants of a SWy-1 smectite and a synthetic dark component.

from other effects cannot be directly used to determine the actual water content of a sample if the nature and chemistry of this sample are unknown. On the contrary, spatial or temporal variability of the parameters of the linear correlation between IBA and continuum reflectance (slope, ordinate origin, and correlation coefficient) could give useful information about the nature of the hydrated materials. First attempts to use this method on the Martian surface by using the OMEGA data set are presented by *Pommerol et al.* [2007] and *Pommerol et al.* [2008].

4.2. How to Deal With the Effect of Particle Size Variations

[93] As discussed earlier in this section, particle size and surface albedo independently influence band strength but the variations of these two parameters are frequently coupled on planetary surfaces. To illustrate how the combined effects of these two parameters influence the IBA criterion, chosen to address the problem of albedo, we plot the evolutions of IBA as a function of continuum reflectance in the case of particle size variations and in the case of granular mixtures of materials with different albedo (Figure 23). These curves are produced by radiative transfer modeling with the optical constants of the SWy-1 smectite. The curves corresponding to granular mixtures are the same than the ones plotted on Figure 13d. The curve corresponding to the effect of particle size is produced by plotting values of the IBA criterion calculated from simulated SWy-1 spectra with different particle sizes as a function of reflectance in the continuum for each spectrum. When particle size decreases, the continuum reflectance increases and so does the IBA criterion. However, the evolution of IBA versus continuum reflectance driven by particle size variations presents different shapes depending on the particle size range. When particle size remains larger than about 100 μm, the relationship between IBA and continuum reflectance is roughly linear because the effect of reflectance continuum variations is dominant. However, the decrease of IBA driven by the reduction of the optical path length when particle size decreases becomes dominant for grains smaller than 100 μm. This particular behavior was already shown for band strength and normalized IBA in section 3. Therefore, the respective influences of particle size and continuum reflectance on IBA will be difficult to discriminate by simply plotting this criterion versus continuum reflectance. An independent way to determine the texture of the surface should be used, if available, to permit a better distinction between these two effects.

[94] From remote sensing, the most efficient way to retrieve planetary surface particle sizes is the use of thermal infrared. Thermal inertia, extracted from temporal variations of surface temperature, is highly correlated with surface material particle size and density [*Presley and Christensen*, 1997]. Successive global maps of the Martian surface thermal inertia have been produced using MGS/TES data [*Putzig et al.*, 2005; *Putzig and Mellon*, 2007]. Therefore, in the case of the Martian surface, it is possible to spatially correlate maps of hydration band strengths (from IRS, ISM, OMEGA, and CRISM data sets) and maps of thermal inertia. However, as surface albedo is the principal cause of hydration band strength variations on the Martian surface [*Jouglet et al.*, 2007], it is necessary to separate the contributions of these two parameters. We propose the use

of diagrams presenting band strength as a function of reflectance continuum on one axis and versus thermal inertia on another axis to allow for a rapid evaluation of the main causes of band strength variations in a particular area. *Pommerol et al.* [2008] applied this method to the OMEGA data set. A decrease of IBA is observed for the lowest values of thermal inertia corresponding to the areas of the Martian surface covered by the finest dust.

5. Conclusion

[95] We have studied the quantitative effects of particle size variations on the H_2O band strength in hydrated minerals and the correlation between band strength and sample albedo. The good consistency between results of physical experiments and radiative transfer modeling indicates that the effects of these parameters are well modeled by the theory of radiative transfer in particulate media. The effects of particle size variations are experimentally studied on three materials, smectite, hydrated volcanic tuff, and immature coal, and numerically studied on a smectite. In agreement with previous studies, we observe that band depth or other simple integrated spectral criteria calculated from reflectance spectra decrease with decreasing particle size for the finest particles. We also show that for the 3-μm band, some criteria like the NIBA are relatively independent of particle size above a threshold size corresponding to the transition between volume and surface scattering. We tested other spectral criteria and concluded that conversion of reflectance spectra to apparent absorbance or single-scattering albedo spectra could lead to dramatic increase of the particle size variation effects on band strength. Mixtures between hydrated materials and a dark material highlight the strong correlation between band strength criteria and sample albedo. Using granular mixtures with different dark component particle size, we are able to isolate the relationship between band strength criteria and albedo independently from the sample water content. We observe a strong linear correlation between IBA at 3 μm calculated from reflectance spectra and sample albedo. This relationship between IBA and continuum reflectance is valid when absorption band is partly saturated or close to saturation. Furthermore, this correlation is valid for any process that alters the sample albedo (granular and spatial mixtures or variations of particle intrinsic optical properties). Therefore, we are relatively confident that a correction to this linear dependence of infrared albedo with band strength (IBA) can be applied on some planetary surfaces. We confirm the conclusion of *Milliken and Mustard* [2007b] that the ESPAT parameter calculated at 2.9 μm is proportional to the sample water content and independent from albedo. However, when the absorption band is saturated at 2.9 μm, ESPAT calculated in the wing of the band at 3.4 μm displays a strong correlation with albedo, especially as albedo decreases below about 0.4. Furthermore, the conversion of reflectance to single-scattering albedo for low values of reflectance seems to induce a general problem of accuracy. The consistency between experiments and numerical models is always good when working with reflectance or apparent absorbance spectra but is dramatically degraded by the highly nonlinear conversion of reflectance to single-scattering albedo. This is a further argument to find a method to correct the correlation between the 3-μm band strength and albedo directly from measured reflectance spectra. If this appears possible for the broad 3-μm band, our results do not indicate a method to correct the correlation between band strength and albedo for the weaker 1.9-μm band. However, the very different shapes of the relationship between the 1.9-μm band strength and continuum reflectance for the various mixing modes (intimate, granular, or geographic) could give an opportunity to identify and discriminate these mixing modes on planetary surfaces.

[96] Correlation of the 1.9-μm band with surface albedo and strong effect of particle size variations on this band and other weak hydration absorption bands in the near infrared probably introduce severe bias in the determination or mapping of hydrated mineralogy on solar system surfaces because detection limits of hydrated minerals are highly dependent on surface texture and cannot be determined if the surface physical properties are unknown. When thermal infrared remote sensing allows the determination of surface thermal inertia, we propose to plot the hydration band strength values as a function of both surface albedo and thermal inertia on two independent axes to allow us to discriminate between the effects of albedo and particle size variations from variations of minerals nature and hydration state. The Martian surface is particularly appropriate to test this method using the linear correlation between the 3-μm band strength and surface albedo. We will apply the conclusions from this study to the OMEGA/Mars Express data set and check if our method is in agreement with results from the method proposed by *Milliken et al.* [2007]. This should also give some answers to the questions raised by *Jouglet et al.* [2007] on the causes of the spatial variations of the water of hydration absorption bands.

[97] **Acknowledgments.** This work has been supported by the French Programme National de Planétologie from CNRS and by the Centre National de Recherches Spatiales. We acknowledge Olivier Brissaud for his assistance in the use of the Spectrogonio radiometer. We thank R. E. Milliken and T. L. Roush for insightful and constructive reviews of this manuscript and R. W. Carlson for helpful editorial and technical comments.

References

Adams, J., and A. Felice (1967), Spectral reflectance 0.4 to 2.0 microns of silicate rock powders, *J. Geophys. Res.*, *72*, 5705–5715, doi:10.1029/JZ072i022p05705.

Aronson, J. R., A. G. Emslie, and H. G. McLinden (1966), Infrared spectra from particulates surfaces, *Science*, *152*, 345–346, doi:10.1126/science.152.3720.345-a.

Bibring, J. P., et al. (2004), OMEGA: Observatoire pour la Minéralogie, l'Eau, les Glaces et l'Activité, in *Mars Express: The Scientific Payload*, edited by A. Wilson, *Euro. Space Agency Spec. Publ.*, *ESA SP-1240*, 37–49.

Bibring, J. P., et al. (2005), Mars surface diversity as revealed by the OMEGA/Mars Express observations, *Science*, *307*, 1576–1581, doi:10.1126/science.1108806.

Bibring, J.-P., Y. Langevin, J. F. Mustard, F. Poulet, R. Arvidson, A. Gendrin, B. Gondet, N. Mangold, P. Pinet, and F. Forget (2006), Global mineralogical and aqueous Mars history derived from OMEGA/Mars Express data, *Science*, *312*, 400–404, doi:10.1126/science.1122659.

Bonnefoy, N. (2001), Développement d'un spectro-goniomètre pour l'étude de la réflectance bidirectionnelle des surfaces géophysiques: Application au soufre et perspectives pour le satellite Io, Ph.D. thesis, Univ. Joseph Fourier, Grenoble, France.

Brissaud, O., B. Schmitt, N. Bonnefoy, S. Douté, P. Rabou, W. Grundy, and M. Fily (2004), Spectrogonio radiometer for the study of the bidirectional reflectance and polarization functions of planetary surfaces: 1. Design and tests, *Appl. Opt.*, *43*, 1926–1937, doi:10.1364/AO.43.001926.

Calvin, W. M. (1997), Variation of the 3-μm absorption feature on Mars: Observations over eastern Valles Marineris by the Mariner 6 infrared spectrometer, *J. Geophys. Res.*, *102*, 9097–9108, doi:10.1029/96JE03767.

Calvin, W. M. (2007), Hydration on Mars: A new method for rapid assessment of extremes, *Lunar Planet.*, *XXXVIII*, Abstract 1390.

Calvin, W. M., and R. N. Clark (1993), Spectral distinctions between the leading and trailing hemispheres of Callisto: New observations, *Icarus*, *104*, 69–78, doi:10.1006/icar.1993.1083.

Carlson, R. W., M. S. Anderson, R. Mehlman, and R. E. Johnson (2005), Distribution of hydrate on Europa: Further evidence for sulfuric acid hydrate, *Icarus*, *177*, 461–471, doi:10.1016/j.icarus.2005.03.026.

Chandrasekhar, S. (1960), *Radiative Transfer*, 2nd ed., 393 pp., Dover, Mineola, N. Y.

Clark, R. N. (1983), Spectral properties of mixtures of montmorillonite and dark grains: Implications for remote sensing minerals containing chemically and physically adsorbed water, *J. Geophys. Res.*, *88*, 10,635–10,644, doi:10.1029/JB088iB12p10635.

Clark, R. N., and T. L. Roush (1984), Reflectance spectroscopy: Quantitative analysis techniques for remote sensing applications, *J. Geophys. Res.*, *89*, 6329–6340, doi:10.1029/JB089iB07p06329.

Clark, R. N., T. V. V. King, M. Klejwa, G. A. Swayze, and N. Vergo (1990), High spectral resolution spectroscopy of minerals, *J. Geophys. Res.*, *95*, 12,653–12,680, doi:10.1029/JB095iB08p12653.

Cooper, C. D., and J. F. Mustard (1999), Effects of very fine particle size on reflectance spectra of smectite and palagonitic soil, *Icarus*, *142*, 557–570, doi:10.1006/icar.1999.6221.

Costanzo, P. M., and S. Guggenheim (2001), Baseline studies of the Clay Minerals Society source clays: Preface, *Clays Clay Miner.*, *49*, 371, doi:10.1346/CCMN.2001.0490501.

de Bergh, C., H. Boehnhardt, M. A. Barucci, M. Lazzarin, S. Fornasier, J. Romon-Martin, G. P. Tozzi, A. Doressoundiram, and E. Dotto (2004), Aqueous altered silicates at the surface of two plutinos, *Astron. Astrophys.*, *416*, 791–798, doi:10.1051/0004-6361:20031727.

Douté, S., and B. Schmitt (1998), A multilayer bidirectional reflectance model for the analysis of planetary surface hyperspectral images at visible and near-infrared wavelengths, *J. Geophys. Res.*, *103*, 31,367–31,390, doi:10.1029/98JE01894.

Erard, S., and W. M. Calvin (1997), New composite spectra of Mars, 0.4–5.7 μm, *Icarus*, *130*, 449–460, doi:10.1006/icar.1997.5830.

Fischer, E. M., and C. M. Pieters (1993), The continuum slope of Mars: Bidirectional reflectance investigations and applications to Olympus Mons, *Icarus*, *102*, 185–202, doi:10.1006/icar.1993.1043.

Gendrin, A., et al. (2005), Sulfates in Martian layered terrains: The OMEGA/Mars Express view, *Science*, *307*, 1587–1591, doi:10.1126/science.1109087.

Guggenheim, S., and A. F. Koster Van Groos (2001), Baseline studies of the Clay Minerals Society source clays: Thermal analysis, *Clays Clay Miner.*, *49*, 433–443, doi:10.1346/CCMN.2001.0490509.

Hapke, B. (1993), *Theory of Reflectance and Emittance Spectroscopy*, Cambridge Univ. Press, Cambridge, U. K.

Hasegawa, S., K. Murakawa, M. Ishiguro, H. Nonaka, N. Takato, C. J. Davis, M. Ueno, and T. Hiroi (2003), Evidence of hydrated and/or hydroxylated minerals on the surface of asteroid 4 Vesta, *Geophys. Res. Lett.*, *30*(21), 2123, doi:10.1029/2003GL018627.

Hunt, G. R. (1982), Spectroscopic properties of rock and minerals, in *Handbook of Physical Properties of Rocks*, vol. 1, edited by R. S. Carmichael, pp. 295–385, CRC Press, Boca Raton, Fla.

Jouglet, D., F. Poulet, R. E. Milliken, J. F. Mustard, J.-P. Bibring, Y. Langevin, B. Gondet, and C. Gomez (2007), Hydration state of the Martian surface as seen by Mars Express OMEGA: 1. Analysis of the 3 μm hydration feature, *J. Geophys. Res.*, *112*, E08S06, doi:10.1029/2006JE002846.

Langevin, Y., F. Poulet, J.-P. Bibring, and B. Gondet (2005), Sulfates in the north polar region of Mars detected by OMEGA/Mars Express, *Science*, *307*, 1584–1586, doi:10.1126/science.1109091.

Le Bras, A., and S. Erard (2003), Reflectance spectra of regolith analogs in the mid-infrared: Effects of grain size, *Planet. Space Sci.*, *51*, 281–294, doi:10.1016/S0032-0633(03)00017-5.

Lyon, R. P. J. (1964), Evaluation of infrared spectroscopy for compositional analysis of lunar and planetary soils, part II: Rough and powdered surfaces, *NASA Contract. Rep., 100*, 262 pp.

Manickavasagam, S., and M. Menguc (1993), Effective optical properties of pulverized coal particles determined from FT-IR spectrometer experiments, *Energy Fuels*, *7*, 860–869.

McCord, T. B., et al. (1999), Hydrated salt minerals on Europa's surface from the Galileo near-infrared mapping spectrometer (NIMS) investigation, *J. Geophys. Res.*, *104*, 11,827–11,851, doi:10.1029/1999JE900005.

Milliken, R. E., and J. F. Mustard (2005), Quantifying absolute water content of minerals using near-infrared reflectance spectroscopy, *J. Geophys. Res.*, *110*, E12001, doi:10.1029/2005JE002534.

Milliken, R. E., and J. F. Mustard (2007a), Estimating the water content of hydrated minerals using reflectance spectroscopy: I. Effects of darkening agents and low-albedo materials, *Icarus*, *189*, 550–573, doi:10.1016/j.icarus.2007.02.017.

Milliken, R. E., and J. F. Mustard (2007b), Estimating the water content of hydrated minerals using reflectance spectroscopy: II. Effects of particle size, *Icarus*, *189*, 574–588, doi:10.1016/j.icarus.2006.12.028.

Milliken, R. E., J. F. Mustard, F. Poulet, D. Jouglet, J.-P. Bibring, B. Gondet, and Y. Langevin (2007), Hydration state of the Martian surface as seen by Mars Express OMEGA: 2. H_2O content of the surface, *J. Geophys. Res.*, *112*, E08S07, doi:10.1029/2006JE002853.

Miyamoto, M., and M. E. Zolensky (1994), Infrared diffuse reflectance spectra of carbonaceous chondrites: Amount of hydrous minerals, *Meteoritics*, *29*, 849–853.

Moroz, V. I. (1964), The infrared spectrum of Mars (1.1–4.1 μm), *Sov. Astron., Engl. Transl.*, *8*, 273–291.

Morris, R. V., W. W. Mendell, and S. C. Neely (1982), Application of Kubelka-Munk theory of diffuse reflectance to geologic problems: The role of scattering, *Geophys. Res. Lett.*, *9*, 113–116, doi:10.1029/GL009i002p00113.

Murchie, S., L. Kirkland, S. Erard, J. F. Mustard, and M. Robinson (2000), Near-infrared spectral variations of Martian surface materials from ISM imaging spectrometer data, *Icarus*, *147*, 444–471, doi:10.1006/icar.2000.6446.

Mustard, J. F., and J. E. Hays (1997), Effects of hyperfine particles on reflectance spectra from 0.3 to 25 μm, *Icarus*, *125*, 145–163, doi:10.1006/icar.1996.5583.

Noe Dobrea, E. Z., J. F. Bell III, M. J. Wolff, and K. D. Gordon (2003), H_2O- and OH- bearing minerals in the Martian regolith: Analysis of 1997 observations from HST/NICMOS, *Icarus*, *166*, 1–20, doi:10.1016/S0019-1035(03)00208-2.

Ockman, N. (1958), The infra-red and Raman spectra of ice, *Philos. Mag.*, *7*, 199–220.

Pieters, C. M. (1983), Strength of mineral absorption features in the transmitted component of near-infrared reflected light: First results from RELAB, *J. Geophys. Res.*, *88*, 9534–9544, doi:10.1029/JB088iB11p09534.

Pommerol, A., B. Schmitt, and J.-P. Bibring (2007), Origins of the spatial variations of the water-of-hydration near-infrared absorption bands observed by OMEGA/Mars Express on the Martian surface, *Lunar Planet.*, *XXXVIII*, Abstract 1787.

Pommerol, A., and B. Schmitt, and the OMEGA Team (2008), Water-of-hydration near-IR bands on Mars: Distinguishing between the effects of hydration state and surface texture using OMEGA and TES datasets, *Lunar Planet.*, *XXXIX*, Abstract 1861.

Poulet, F., J.-P. Bibring, J. F. Mustard, A. Gendrin, N. Mangold, Y. Langevin, R. Arvidson, B. Gondet, and C. Gomez (2005), Phyllosilicates on Mars and implications for early Martian climate, *Nature*, *438*, 623–627, doi:10.1038/nature04274.

Presley, M. A., and P. R. Christensen (1997), The effect of bulk density and particle size sorting on the thermal conductivity of particulate materials under Martian atmospheric pressures, *J. Geophys. Res.*, *102*, 9221–9230, doi:10.1029/97JE00271.

Putzig, N. E., and M. T. Mellon (2007), Apparent thermal inertia and the surface heterogeneity of Mars, *Icarus*, *191*, 68–94, doi:10.1016/j.icarus.2007.05.013.

Putzig, N. E., M. T. Mellon, K. A. Kretke, and R. E. Arvidson (2005), Global thermal inertia and surface properties of Mars from the MGS mapping mission, *Icarus*, *173*, 325–341, doi:10.1016/j.icarus.2004.08.017.

Quirico, E., S. Douté, B. Schmitt, C. de Bergh, D. P. Cruikshank, T. C. Owen, T. R. Geballe, and T. L. Roush (1999), Composition, physical state and distribution of ices at the surface of Triton, *Icarus*, *139*, 159–178, doi:10.1006/icar.1999.6111.

Rivkin, A. S., J. K. Davies, J. R. Johnson, S. L. Ellison, D. E. Trilling, R. H. Brown, and L. A. Lebofsky (2003), Hydrogen concentrations on C-class asteroids derived from remote sensing, *Meteorit. Planet. Sci.*, *38*, 1383–1398.

Rivkin, A. S., L. A. McFadden, R. P. Binzel, and M. Sykes (2006), Rotationally-resolved spectroscopy of Vesta I: 24 μm region, *Icarus*, *180*, 464–472, doi:10.1016/j.icarus.2005.09.012.

Roush, T. L. (2005), Near-infrared (0.67–4.7 μm) optical constants estimated for montmorillonite, *Icarus*, *179*, 259–264, doi:10.1016/j.icarus.2005.06.004.

Ryskin, Y. (1974), The vibrations of protons in minerals: Hydroxyl, water and ammonium, in *The Infrared Spectra of Minerals*, edited by V. C. Farmer, pp. 137–182, Mineral. Soc., London.

Salisbury, J. W., and A. D. Wald (1992), The role of volume scattering in reducing spectral contrast of reststrahlen bands in spectra of powdered minerals, *Icarus*, *96*, 121–128, doi:10.1016/0019-1035(92)90009-V.

Salisbury, J. W., and L. S. Walter (1989), Thermal infrared (2.5–13.5 (μm) spectroscopic remote sensing of igneous rock types on particulate plane-

tary surfaces, *J. Geophys. Res.*, *94*, 9192–9202, doi:10.1029/JB094iB07p09192.

Sato, K., M. Miyamoto, and M. E. Zolensky (1997), Absorption bands near 3 microns in diffuse reflectance spectra of carbonaceous chondrites: Comparison with asteroids, *Meteorit. Planet. Sci.*, *32*, 503–507.

Shkuratov, Y. G., and Y. S. Grynko (2005), Light scattering by media composed of semitransparent particles of different shapes in ray optics approximation: Consequences for spectroscopy, photometry, and polarimetry of planetary regoliths, *Icarus*, *173*, 16–28, doi:10.1016/j.icarus.2003.12.022.

Shkuratov, Y. G., L. Starukhina, H. Hoffman, and G. Arnold (1999), A model of spectral albedo of particulate surfaces: Implications for optical properties of the Moon, *Icarus*, *137*, 235–246, doi:10.1006/icar.1998.6035.

Van Keulen, L. M., T. B. McCord, G. B. Hansen, C. A. Hibbitts, and J. K. Crowley (2000), The effect of grain size on the near-infrared reflectance spectra of some hydrated salt minerals, *Lunar Planet. Sci.*, *XXXI*, Abstract 1539.

Vilas, F., S. M. Lederer, S. L. Gill, K. S. Jarvis, and J. E. Thomas-Osip (2006), Aqueous alteration affecting the irregular outer planets satellites: Evidence from spectral reflectance, *Icarus*, *180*, 453–463, doi:10.1016/j.icarus.2005.10.004.

Whiting, M. L., L. Li, and S. L. Ustin (2004), Predicting water content using Gaussian model on soil spectra, *Remote Sens. Environ.*, *89*, 535–552, doi:10.1016/j.rse.2003.11.009.

Yen, A. S., B. C. Murray, and G. R. Rossman (1998), Water content of the Martian soil: Laboratory simulations of reflectance spectra, *J. Geophys. Res.*, *103*, 11,125–11,134, doi:10.1029/98JE00739.

A. Pommerol and B. Schmitt, Laboratoire de Planétologie de Grenoble, Université Joseph Fourier, CNRS/INSU, Bâtiment D de Physique, B. P. 53, F-38041, Grenoble CEDEX 9, France. (antoine.pommerol@obs.ujf-grenoble.fr)